Geochemistry, Geophysics, Geosystems®

RESEARCH ARTICLE
10.1029/2023GC011282

A Hyperactive Geomagnetic Field in the Late Visean (Early Carboniferous) From the Late Asbian Stratotype Section in Northwest England, UK

Mark W. Hounslow[1,2], Andrew J. Biggin[2], Pedro Cózar[3], Ian D. Somerville[4], Tereza Kamenikova[1], and Courtney J. Sprain[5]

[1]Lancaster Environment Centre, Lancaster University, Lancaster, UK, [2]Earth, Ocean and Ecological Sciences, University of Liverpool, Liverpool, UK, [3]Instituto de Geociencias (CSIC-UCM), Madrid, Spain, [4]UCD School of Earth Sciences, University College Dublin, Dublin, Ireland, [5]Department of Geological Sciences, University of Florida, Gainesville, FL, USA

Key Points:

- A 195 m section, representing ~2 Myr, yields a magnetostratigraphy comprizing nine major magnetozone couplets and seven submagnetozones
- Primary magnetizations are predominantly carried by hematite with lesser important detrital magnetite. Data pass regional fold tests
- A reversal frequency of 15.7 ± 0.75 Myr^{-1} is calculated, suggesting that the geodynamo was in a hyperactive state at ~333 Ma

Supporting Information:

Supporting Information may be found in the online version of this article.

Correspondence to:

M. W. Hounslow,
m.hounslow@lancaster.ac.uk

Citation:

Hounslow, M. W., Biggin, A. J., Cózar, P., Somerville, I. D., Kamenikova, T., & Sprain, C. J. (2024). A hyperactive geomagnetic field in the late Visean (Early Carboniferous) from the late Asbian stratotype section in northwest England, UK. *Geochemistry, Geophysics, Geosystems*, *25*, e2023GC011282. https://doi.org/10.1029/2023GC011282

Received 6 OCT 2023
Accepted 2 MAR 2024

Author Contributions:

Conceptualization: Mark W. Hounslow, Andrew J. Biggin
Data curation: Mark W. Hounslow
Formal analysis: Mark W. Hounslow, Pedro Cózar, Ian D. Somerville, Tereza Kamenikova, Courtney J. Sprain
Funding acquisition: Mark W. Hounslow, Andrew J. Biggin
Investigation: Mark W. Hounslow, Pedro Cózar, Ian D. Somerville, Tereza Kamenikova, Courtney J. Sprain

Plain Language Summary Nearly synchronous global changes in geomagnetic polarity give both a detailed irregular pacing to geological time and provide a glimpse into heat transfer processes across the core—mantle boundary which drives the Earth's geodynamo. Although the Late Carboniferous is characterized by some well-studied reversals, details of the tempo of polarity changes in the Early Carboniferous are unknown. This work addresses this by providing a detailed record of polarity changes over a ~2 million year interval at around 334.5–332.5 million years ago-from the Trowbarrow Quarry section in NW England. We demonstrate that these limestones likely preserve magnetization from close to their time of formation and record at least 31 polarity reversals. These observations support the idea that the Earth's dynamo was in a hyperactive reversing state similar to those sustained for tens of Myr in the Late Jurassic, parts of the Cambrian and the Late Ediacaran. It further corroborates a ~200 Myr cyclicity in paleomagnetic field behavior since the Precambrian, potentially linked to variable core heat flow forced by mantle convection.

Abstract The pattern of geomagnetic polarity changes during the Early Carboniferous (Mississippian) is not known in detail. This information sparsity is addressed by determining a magnetostratigraphy from the late Asbian (late Visean at ~333 Ma) in Trowbarrow Quarry, UK. This is the stratotype section of the late Asbian and has a detailed foraminiferal zonation based on the same set of paleomagnetic samples, establishing a detailed biostratigraphy. The 195 m-thick section was sampled at an average spacing of 1.1 m, yielding a detailed magnetostratigraphy comprising nine major magnetozone couplets, and seven submagnetozones. The section dataset has a 78% bias to normal polarity determined from 177 sampling levels. The magnetization is carried by a mixture of hematite and detrital magnetite, with 68% of specimens dominated by hematite magnetizations. The primary magnetization passes a fold test showing its age was prior to the latest Carboniferous. The hematite is inferred to be largely of detrital, eolian origin, although some reddened levels are associated with emergent surfaces, suggesting that a small fraction of hematite is associated with platform emergence. The Mississippian age magnetization is partly overprinted with Kiaman Superchron-age and Brunhes-age magnetizations. Using the duration of the section based on astrochronology indicates a reversal frequency of 15.7 ± 0.75 Myr^{-1}, indicating that the geodynamo was in a hyperactive reversing state between 335 and 333 Ma.

1. Introduction

Stratigraphic changes in geomagnetic polarity (magnetostratigraphy) have become one of the standard tools for stratigraphic study in the Mesozoic and Cenozoic, allowing environmental changes to be calibrated to precise time intervals (Hounslow et al., 2022; Miller & Wright, 2017; Nie et al., 2020). For much of the Pennsylvanian (Late Carboniferous), progress has been made in defining a polarity timescale (Opdyke & DiVenere, 2004; Opdyke et al., 2014), but details require validation, with those currently available largely based on few age-overlapping studies (Hounslow, 2022). In the Carboniferous, regional differences in stratigraphic scales and biozonations contribute to additional uncertainty in how to correlate between the various studies when compiling a composite global polarity scale (Hounslow, 2022). For much of the Early Carboniferous (Mississippian) and Devonian, changes in geomagnetic polarity are not known in detail or those intervals that have been studied are open to additional uncertainty (Green et al., 2021; Van der Boon et al., 2022).

Methodology: Mark W. Hounslow, Tereza Kamenikova
Project administration: Mark W. Hounslow, Andrew J. Biggin
Resources: Mark W. Hounslow
Software: Mark W. Hounslow
Validation: Mark W. Hounslow, Pedro Cózar
Visualization: Mark W. Hounslow
Writing – original draft: Mark W. Hounslow, Andrew J. Biggin, Pedro Cózar, Ian D. Somerville, Tereza Kamenikova
Writing – review & editing: Mark W. Hounslow

In addition to their applications in stratigraphy, quantification of geomagnetic reversal rates provides clues to the workings of the geodynamo, evolution of the core and its interaction with the mantle (Biggin et al., 2012; Davis & Buffett, 2022; Hounslow et al., 2018). In the Paleozoic and Ediacaran, intervals of hyperactivity in reversal rates (rates >8 Myr^{-1}) seem to be common features (Gallet et al., 2019), along with intervals which do not conform to expectations of the bipolar behavior of the geomagnetic field (Pavlov et al., 2018; Van der Boon et al., 2022). The age distribution of such unusual behavior is also poorly known. For these reasons, it is important to enhance our understanding of geomagnetic polarity changes in the mid Paleozoic (Silurian-Devonian and Mississippian), which is the least well understood interval in this context, since the early Ediacaran.

This work addresses the paucity of magnetostratigraphic records in the Visean (~347–330 Ma), which is addressed here by data from the late Asbian (~333 Ma), which is a regional substage of the late Visean defined in Britain. The Visean has no internationally agreed subdivisions, yet formal regional divisions exist (Figure 1). In parallel, we have also improved our understanding of the international correlation of the late Asbian and the older Holkerian substages (Cózar et al., 2022a, 2022b, 2023a). We detail here the magnetostratigraphy of the Trowbarrow Quarry section in NW England, UK (Figure 2), which is the stratotype section for the late Asbian (Cózar et al., 2022b), and is also important as a reference section for the apparently synchronous emergent surfaces in carbonate platforms which punctuate the late Asbian in western Europe (Cózar et al., 2022c). These emergent

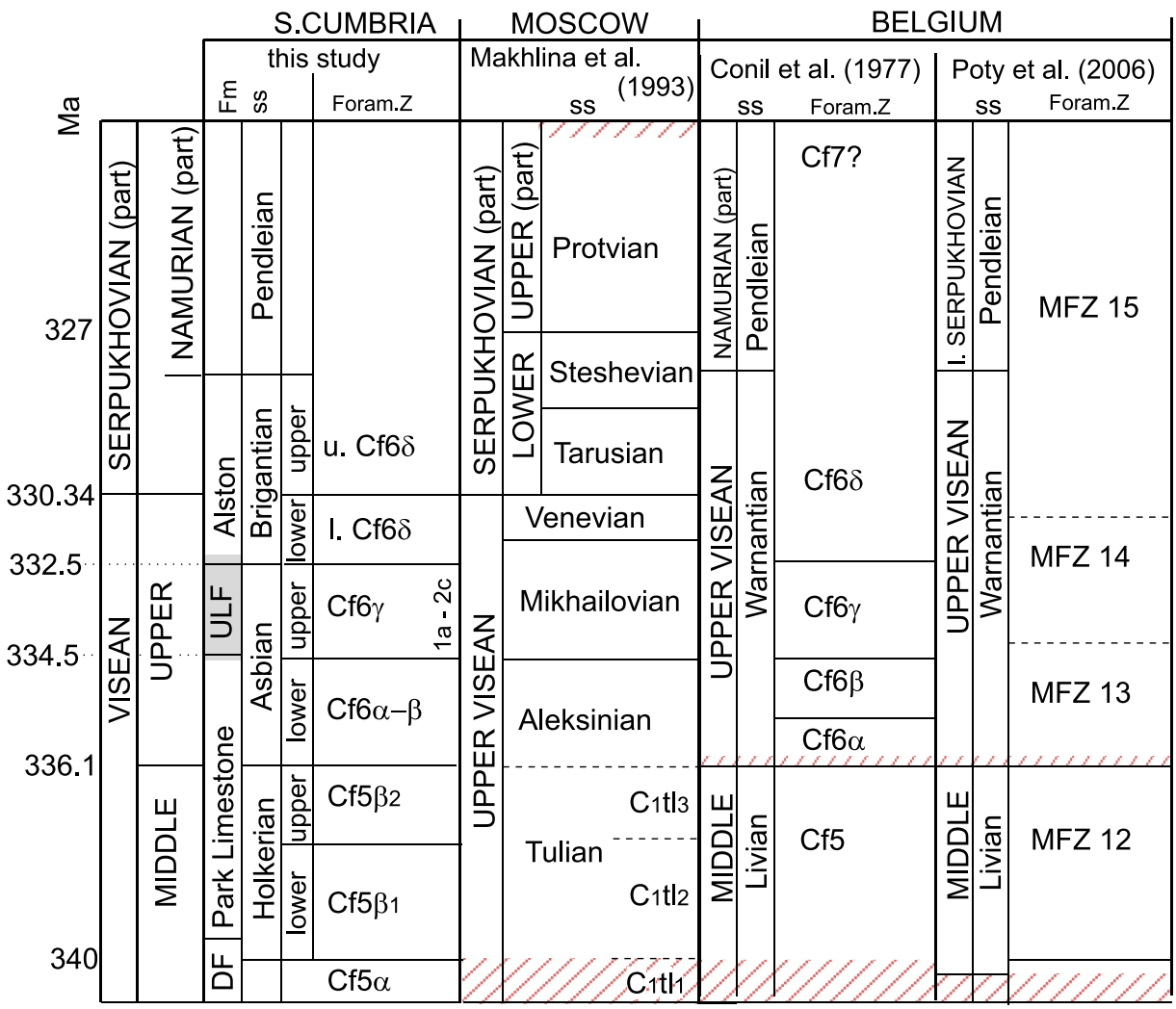

Figure 1. The foraminiferal zonations and British substages in south Cumbria (and North Lancashire), and comparable zonations and regional substages in some other key locations for the Visean. Hatching = missing intervals. Fm = formations, ss = regional substages, MFZ = Mississippian foraminiferal Zones, Foram.Z = biozones and subzones, DF = Dalton Formation, ULF = Urswick Limestone Formation. Grayed interval is the part studied here at Trowbarrow Quarry. Million years (Ma) ages from Pointon et al. (2014); Aretz et al. (2020), and Hounslow, Cózar, et al. (2024).

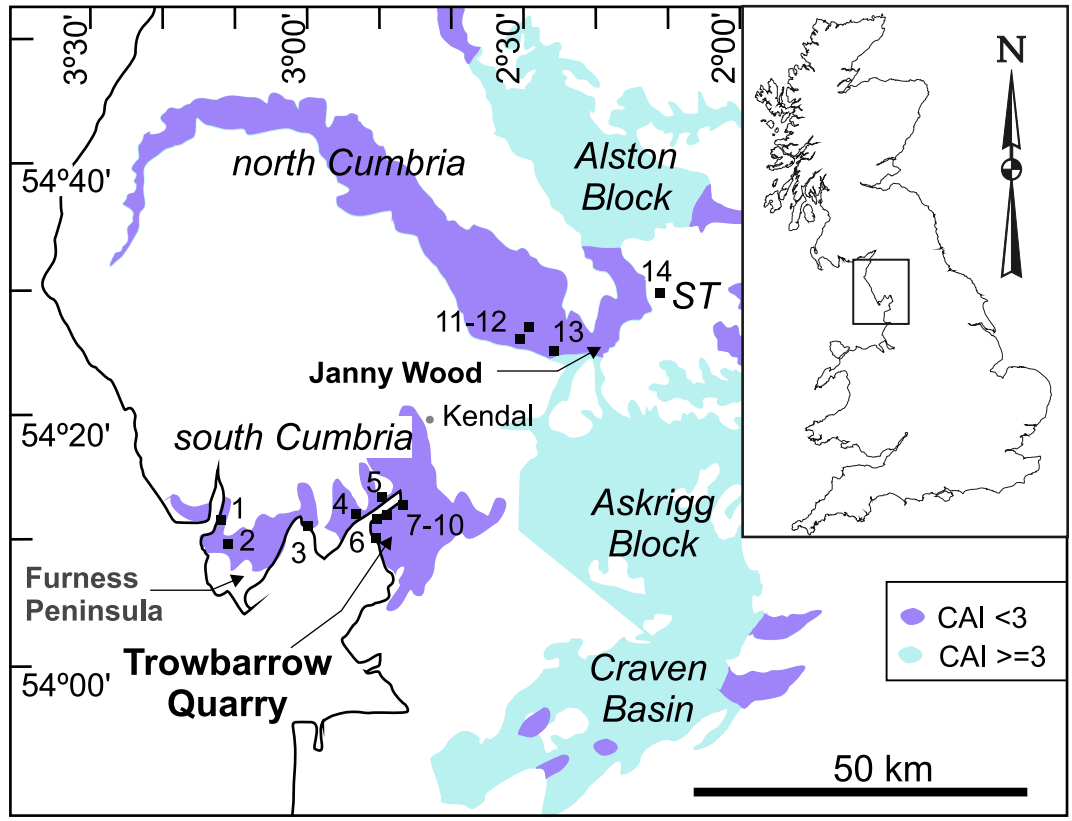

Figure 2. Distribution of Visean age sediments and the distribution of conodont alteration indices (CAI) thresholded at the CAI = 3 level (CAI data from Burnett, 1987; Metcalfe & Riley, 2010). Also labeled are the basins and blocks in northwest England. CAI data in south Cumbria-NW Lancashire are largely absent and are assumed to be similar to that in north Cumbria. Numbered localities relate to the additional sample set, are: 1 = Dunnerholme Point, 2 = Dalton in Furness road cuttings, 3 = Barker Scar, 4 = Meathop Quarry, 5 = Whitescar Quarry, 6 = Jenny Browns Point, 7 = Grubbins Wood, 8 = Coastguard Quarry, 9 = Sandside railway cutting, 10 = Sandside Quarry, 11 = Ashfell Edge road cutting, 12 = Little Asby Scar, 13 = Ravenstonedale River. 14 = Mouse Gill (details in Table S1 in Supporting Information S1). ST = Stainmore Trough.

surfaces are thought to be related to glacioeustatic fluctuations in sea-level, initiated near the base of the late Asbian. We also examine Visean age units at other localities in south and northeast Cumbria to test the relative age of the magnetization with respect to folding (Figure 2).

1.1. Geological Background

This work is largely focused on the Urswick Limestone Formation (Figure 1), although our magnetostratigraphic study overlaps with the top of the underlying Park Limestone Formation and the basal few meters of the overlying Alston Fm in Trowbarrow Quarry (Cózar et al., 2022b). The Urswick Limestone Fm is restricted to south Cumbria and northern-most Lancashire (the South Cumbria Shelf; Figure 2) but has coeval equivalents to the east in the Craven Basin, the Askrigg and Alston blocks (Waters et al., 2017, 2021), and north Cumbria (Waters et al., 2011a) (Figures 1 and 2).

The Urswick Limestone Fm is a carbonate ramp succession, which passes southwards into the eastern Irish Sea Basin where more shale-rich successions occur, continuous with coeval successions in the Craven Basin (Wakefield et al., 2016). Within the South Cumbria Shelf, the regional facies changes within the Urswick Limestone Fm are generally well understood through the work of Horbury (1987, 1989), Horbury and Adams (1996), and Adams et al. (1990). A detailed foraminiferal zonation has allowed clear identification of the base of the late Asbian and the base of the Brigantian (Cózar et al., 2022b; Figure 1). The latter faunal records can be clearly related to the Brigantian boundary stratotype at Janny Wood (Figure 2), 55 km to the NE (Cózar et al., 2023b; Cózar & Somerville, 2004, 2005). The Trowbarrow foraminiferal biozonation is based on the same

set of paleomagnetic samples described here. Although a hiatus has commonly been inferred at the base of the Urswick Limestone Fm (Adams et al., 1990; Waters et al., 2021), this cannot be demonstrated with biostratigraphy, which suggests (at least at Trowbarrow Quarry) that the basal succession is complete, and any truncation is no greater than at other similar paleokarsts in the Urswick Limestone Fm. The inference of this substantial unconformity is in part related to the prior inadequacy of the biostratigraphic definition of the early Asbian (Cózar et al., 2022b).

We have also evaluated samples from fourteen other localities (1–14 in Figure 2) in Cumbria and north Lancashire to provide data for a regional tilt test. These localities range in age from the latest Tournaisian to late Visean (~347–332 Ma) with locality 14 in the Namurian at ~325 Ma (Figure 2, details in Table S1 in Supporting Information S1). Here, the late Tournaisian-Visean successions rest unconformably on folded Ordovician-Silurian clastic successions, both of which are affected by extensional faulting, giving east- and south-directed tilted fault blocks in south Cumbria, and north and northeast tilting in NE Cumbria. This faulting is possibly partly of Late Pennsylvanian age (Waters et al., 1994), although more likely, largely related to extension in the Irish Sea Basin during the Permian-Triassic (Johnson et al., 2001). At present, the Late Permian and Triassic rock rests unconformably on the Carboniferous. In the South Cumbria Shelf area, earlier E-W compression produced some compressional structures and gentle folding, probably related to basin inversion in the Late Pennsylvanian to Early Permian.

The Trowbarrow Quarry is situated within one of these compressional structures, an east-facing monocline, N-S oriented, like the Hutton monocline to the east (Brandon et al., 1998). Late Pennsylvanian basin inversion is a more widespread feature of the Craven Basin (Fraser & Gawthorpe, 2003; Waters et al., 1994), possibly coeval with maximum burial of the Visean successions (Metcalfe & Riley, 2010). In south Cumbria, Late Pennsylvanian-Early Permian uplift may have been of the order of 1.5 km or more (Johnson et al., 2001).

1.2. Previous Paleomagnetic Studies in the Visean in Britain and Ireland

Paleomagnetic and magnetostratigraphic studies of Visean volcanic units in the Scottish Midland Valley and Derbyshire have yielded magnetization interpreted to be primary (Wilson & Everitt, 1963; Torsvik et al., 1989; Rother & Storetvedt, 1991; Piper et al., 1991; magnetostratigraphy detailed in Hounslow, 2022), data which has also been widely used in apparent polar wander path construction (Torsvik et al., 2012). Studies on Visean limestones have been less successful due to a strong reverse polarity remagnetization acquired during the interval of the Kiaman Superchron (Late Pennsylvanian- Middle Permian in age), which dominates in many British and Irish Visean age limestones (McCabe & Channell, 1994; Morris, 1972; Wilkinson et al., 2017).

In Britain, early paleomagnetic studies of the Lower Carboniferous focussed on the Craven Basin and Askrigg Block successions (Turner, 1975; Turner et al., 1979; Turner & Tarling, 1975) and largely used spinner magnetometers. These were likely insufficiently sensitive to precisely define the sometimes-weak primary magnetization of these limestones. Nevertheless, the hypothesis of complete re-magnetization of the British Visean limestones advocated by McCabe and Channell (1994) is an over-simplification, since prior measurements clearly showed dual polarity magnetization (Turner et al., 1979; Turner & Tarling, 1975), including downwards-directed SSW magnetization (after tilt corrections), similar to those observed from Visean-age volcanics (Addison et al., 1985; Turner et al., 1979). Even the earliest studies on Irish Visean limestones hinted at the presence of inadequately resolved high-stability components, in addition to the lower-stability Kiaman-age directions isolated during thermal demagnetization (Morris, 1971). Furthermore, in the measurements of McCabe and Channell (1994) from the early Visean and Asbian of the Craven Basin, the characteristic directions have southerly positive and negative inclination groupings with respect to the bedding plane, implying that these "re-magnetizations" are potentially not from a single age interval in the Late-Carboniferous to Permian.

Studies of conodont alteration indices (CAI) have shown that Visean successions in the Craven Basin have CAI values of 2.5–3.5, largely related to maximum burial during the Late Pennsylvanian in the Craven Basin (Metcalfe & Riley, 2010). A CAI value of three corresponds to a possible burial temperature of 110–120°C with assumed geothermal gradient of 30°C/km and 30 Myr burial (Metcalfe & Riley, 2010). On the Askrigg and Alston blocks (Figure 2), larger CAI values of 3–4 occur due to the higher geothermal gradients than in other areas (Burnett, 1987). In the study area, changes in CAI are not known to be related to mineralization or igneous activity. Using both the evidence of some potentially primary magnetization in these limestones, and lower CAI values on the flanks of Cumbria we focussed our study on the areas with lower CAI (Figure 2). CAI values are

scarcely known from south Cumbria, with a single CAI value of 2 from the Urswick Limestone Fm near Kendal (Burnett, 1987), and CAI values are assumed to be like the better-studied Visean of northern Cumbria, with a similar burial and uplift history to the South Cumbria Shelf (Kirby et al., 2000; Mitchell et al., 1978). A CAI value of two corresponds to a likely burial temperature of ~80°C for 30 Myr (Burnett, 1987).

2. Methods and Sampling

2.1. Sampling and Section Details

The main activity was focussed on the Trowbarrow quarry section, where oriented samples were collected with an average stratigraphic spacing of 1.1 m (Figures S1–S3 in Supporting Information S1). These were exclusively hand samples, on which a flat surface was made with a diamond-cup grinder, and oriented using a foot-print style orientation device (Hounslow et al., 2022). Drilling was not allowed at this protected SSSI site. The remaining parts of the samples were used for foraminiferal and petrographic study (detailed in Cózar et al., 2022b) and rock magnetic study. The bedding at Trowbarrow is near vertical and slightly overturned throughout the section (Figure S1 and further details in Supporting Information S1).

Lithologies sampled in the section range from carbonate mudstones to wackestones, packstones and grainstones. Shale intervals and the silty tops of paleosols could not be sampled. Some reddened levels are associated with the emergent surfaces, and 12 samples are in close proximity to these reddened surfaces. Dolomitization is insignificant in this section. However, some emergent surfaces and their paleosols are associated with gray intervals, likely due to the type of paleosol pyritization described by Wright et al. (1997).

Samples from the additional localities 1 to 14 were collected in a similar way (referred to as the "additional set" here), with one to four samples from each locality (details in Table S1 in Supporting Information S1). These localities include a variety of bedding dips, from shallow to steep dips (i.e., localities 7, 8, 14) to evaluate a regional tilt test, in combination with the data from Trowbarrow (bedding dips at Trowbarrow are not sufficiently varied to evaluate an individual fold test). The additional samples were predominantly limestones, and dolomitized limestones, but included some red and brown sandstones (localities 2, 14).

2.2. Paleomagnetic Methods

Measurements of Natural Remanent Magnetization (NRM) were made using a 3-axis 2G Enterprises RAPID cryogenic magnetometer at Lancaster University, which has a noise floor ~2×10^{-12} A.m^2 (~0.3 μA/m; with holder correction). The magnetometer was housed in a large Helmholtz cage for field cancellation, which together with the Mu-metal shields reduced the Earth's magnetic field to around 0.03–0.08 μT at the demagnetizer coil position. Specimen magnetization measurements were performed using a "measurement blank" (i.e., a blank subjected to all the same steps). This bypassed the RAPID "standard holder-correction procedure." The GM4Edit software was used for the blank-type corrections to the data (Hounslow, 2019). Holder magnetizations for NRM measurements have a median of 3.5×10^{-12} A.m^2 ($1\sigma = 7 \times 10^{-12}$ A.m^2). The additional set was measured at Liverpool University, using a similar magnetometer and set-up (but standard holder removal) with a noise floor ~1×10^{-11} A.m^2 (~1 μA/m; with holder correction) and median holder magnetization of 13×10^{-12} A.m^2 ($1\sigma = 36 \times 10^{-12}$ A.m^2; data based on these measurements).

Some specimens were subjected to stepwise thermal demagnetization, using a Magnetic Measurements Ltd, MMTD1 thermal demagnetizer, in 100–50°C steps up to 700°C. Magnetic susceptibility measurements (using a Bartington MS2 meter, at 0.47 kHz) were performed after each heating step to monitor mineralogical changes caused by the heating, which were often a major problem. Many specimens were measured by a combination of thermal demagnetization up to around 250–400°C followed by static AF demagnetization on the RAPID (up to 95 mT). This combined procedure limited thermal alteration, which often obscured the characteristic remanent magnetization (ChRM). This alteration limited the useful upper limit to thermal demagnetization for many samples. No specimens were measured using AF only. Specimens were held in Mu-metal shielded boxes and larger Mu-metal shields between measurements. At Lancaster University, from the 30 mT AF step onwards, the GRM corrections procedure (ZD-method) of Stephenson (1993) was applied to all data to limit the impact of GRM acquisition. Post-processing of these data was applied using GM4Edit software (Hounslow, 2019). Liverpool University used the standard RAPID set-up and demagnetization (static AF to 95 mT), but many of the

weaker samples were inverted and re-measured to improve accuracy. Many were also tumble-demagnetized up to 200 mT on an AGICO demagnetizer.

The specimen demagnetization results were analyzed using principal component analysis using LINEFIND (Kent, 1985) as a DOSbox version (Hounslow, 2023a). LINEFIND is more sophisticated than conventional analysis (Heslop & Roberts, 2016; McFadden & Schmidt, 1986), since it has statistical tests for linearity and planarity, uses a fitted model of the measurement variance, and determines α_{95} of lines and planes rather than maximum angular deviation values. A tuning parameter (ρ) is used in combination with visual interpretation and Akaike's information criteria in selecting ρ (details in Kent, 1985; McFadden & Schmidt, 1986; Hounslow, 2023a). Great circle type behavior was seen in many specimens during demagnetization, and behavioral classes S (for linear line fits) and T (great circle behavior) were assigned to specimens (like used by Montgomery et al. (1998) and Hounslow et al. (2004)). These were further sub-divided into three qualitative classes (S1, S2, S3 and T1, T2, T3; with class 1 the top quality). For S-class behavior, the directional scatter and length of the fitted line (in the Zijderveld projections) were used for qualitative classification. For T-class behavior, the scatter and approach to the expected ChRM direction was used, with the T1 class having a closer approach but without reaching a stable endpoint (illustrative examples in Figure S8 in Supporting Information S1). The relationship of these qualitative classes to the α_{95} of the S-class lines and T-class poles to the great circles is shown in Figure 3a. Directional data for 1.8% of the weakest intensity specimens (often <1 μA/m) was too erratic, and these were assigned as unused data (X-class). This X-class was also assigned to specimen data in which alteration during thermal demagnetization totally obscured the ChRM (3.8% of specimens).

For the specimens from Trowbarrow, virtual geomagnetic pole (VGP_R) latitudes (Hounslow et al., 2022) were determined with respect to the mean VGP direction (S-class data sets) for sub-divisions of the section in Table 1. Values of VGP_R latitude near +90° indicate a specimen with normal polarity and values near −90° indicate a reversed polarity specimen. In addition to reversal tests (McFadden & McElhinny, 1990), the site mean VGP $A95_{min}$ and $A95_{max}$ thresholds of Deenen et al. (2014) were used as a measure of the capture of secular variation in the directional datasets. Based on the approach to expected Carboniferous directions and the qualitative confidence attached to that polarity inference, specimens were also assigned a polarity quality class R, R?, R??, N??, R??,N??,N? or N, to indicate either reversed or normal polarity status. R? or N? indicate a polarity assignment of middle quality, compared to R or N of top quality, and R??, N?? of lowest quality. A class of "?" indicates a specimen could not confidently be assigned a polarity. The relationships of the VGP_R latitude and polarity classifications to the demagnetization behavior classes are shown in Figures 3b–3d.

2.3. Rock Magnetic Methods

For the Trowbarrow set, magnetic mineralogy was investigated using one sister specimen from each sampled horizon. This used static anhysteretic remanent magnetization (ARM) imparted with a 100 μT DC field, and 80 mT AF field and subsequently its static AF demagnetization at 40 mT on the RAPID (all along Z-axis only). The hardness of the ARM (Peters & Thompson, 1998) was calculated as $\%d.ARM_{40mT} = 100*(ARM_{-40mT}/ARM80_{mT})$. The RAPID blank-type corrections remove the ARM magnetization and demagnetization of the quartz glass rod during these experiments. Subsequently determined on the same specimen was isothermal remanent magnetization (IRM) at 1000 mT, with 40, 100, 300 and 1000 mT backfield measurements to determine the S-ratio ($-IRM_{0.1T}/IRM_{1T}$), the HIRM (IRM_{1T}-$IRM_{0.3T}$) and the coercivity of remanence (B_{cr}) was estimated by linear interpolation. IRM was measured on a JR6 spinner magnetometer (with cross calibrated intensity to the RAPID) using procedures in Walden (1999). Also, rotational remanent magnetization (RRM) and rotational ARM (ARM_{ROT}) were measured on nine specimens at a rotation rate of 2.5 Hz, using the procedures in Hounslow et al. (2023) to characterize the single domain (SD) magnetic mineralogy. In these cases, the diagnostic indicator determined is the effective gyromagnetic field Bg. The RRM of two of these specimens could not be reliably measured. Two specimens from the additional set were investigated with a Quantum Design Magnetic Properties Measurement System (MPMS-5S) at the Institute for Rock Magnetism at the University of Minnesota (detailed in Figure S5 in Supporting Information S1). Additional details of the stratigraphic variation of the rock magnetic data at Trowbarrow are in Hounslow, Cózar, et al. (2024). A subset of the Trowbarrow samples were measured for carbon isotopes to aid in the longer-term correlation to other sections without such a detailed foraminiferal biostratigraphy (Figure S4; details in Supporting Information S1).

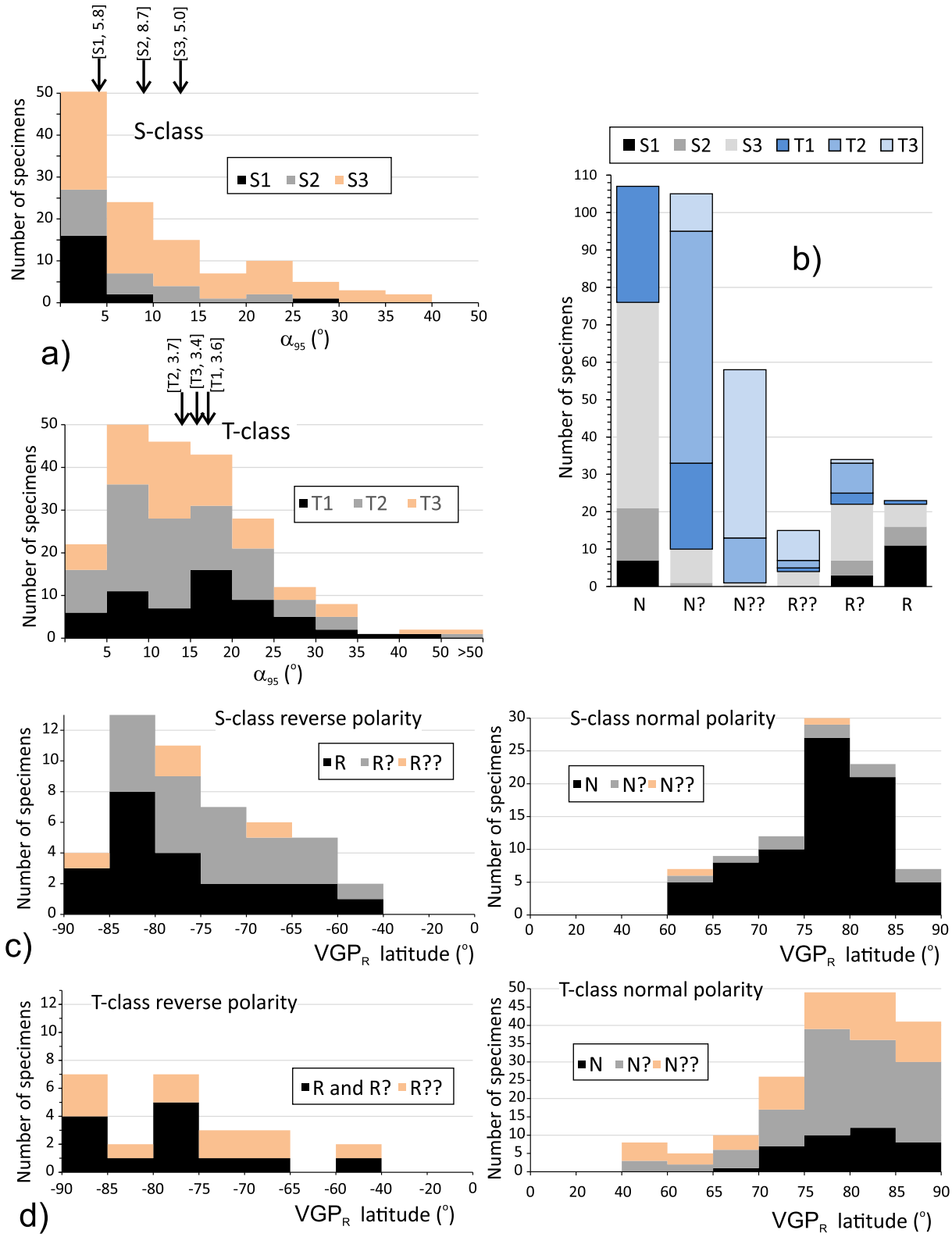

Figure 3. For the Trowbarrow dataset: (a) the partition of LINEFIND α_{95} values with demagnetization behavioral classes, (b) the partition of demagnetization classes with polarity quality, and (c) and (d) the partition of reverse and normal polarity quality classes with VGP_R latitude. Similar data for the additional set are shown in Figure S7 in Supporting Information S1. S1, S2, S3 are descending quality classes of PCA lne fits, and T1, T2, T3 are descending quality classes of great circle PCA fits. Arrows in (a) are the mean α_{95}, and the mean ρ value of the respective class.

Table 1
Trowbarrow Quarry Directional Means (With Tectonic Correction and Converted to Normal Polarity), Reversal Tests and South VGP Poles

Type/section/Unit	Dec(°)	Inc(°)	K/α_{95}(°)	Ns/Nl/Np	Reversal test	G_o/G_c(°)	Plat/Plong(°)	Dp/Dm (°)	A95 (min, max)
Humphrey Head Lmst Mb- Peghorn Lmst Mb									
Line fits[a]	30.7	−29.8	29.4/8.6	9/11/0	Ro-	11.6/30	−15.1/327.0	5.3/9.5	8.9 (5,21)
Locality mean[b]	34.1	−22.4	35.5/5.0	23/11/36	Ro	4.9/24	−18.1/322.2	2.8/5.3	4.3 (3.4,11.4)
Upper Urswick Limestone									
Line fits[a]	36.1	−29.3	23.1/3.1	64/93/0	R-	9.9/6.5*	−13.7/321.8	1.9/3.4	3.3 (2.3,6)
Locality means[b]	34.1	−27.5	38.3/2.3	101/93/111	Rc	5.5/10	−15.3/323.2	1.4/2.5	2.1 (1.9, 4.5)
Lower Urswick Limestone									
Line fits[a]	38.0	−27.4	26.1/5.2	22/31/0	R-	13.5/9.4*	−14.3/319.7	3.1/5.8	5.3 (3.5,11.7)
Locality means[b]	34.7	−25.3	35.8/3.3	52/31/71	Rb	5.1/7.7*	−16.4/322.3	1.9/3.6	2.7 (2.5,6.8)
Trowbarrow section									
Line fits[a]	36.1	−28.9	24.2/2.5	95/135/0	R-	10.1/5.1*	−14.1/319.6	3.1/5.7	2.6 (1.9, 4.7)
Locality means[b]	34.3	−26.1	36.9/1.8	176/135/218	R-	4.5/4.3	−16.1/322.8	1.1/2.0	1.5 (1.5,3.2)
Other Visean localities									
GC means[c]	36.6	−31.2	12/5.1	30/14/30	Rc	12.9/13.1	–	–	–
Locality means[a]	36.6	−31.2	29.7/4.9	30/14/30	Rc	4.9/10.4	−12.1/321.7	–	4.6 (3.1, 9.6)

Note. Ns = number of levels (sites), Nl = number of specimens used with fitted lines, and Np = number of specimens with great circle planes used in the determining the mean direction. α95, Fisher 95% cone of confidence. *k*, Fisher precision parameter. G_o is the angular separation between the inverted reverse and normal directions, and G_c is the critical value for the reversal test. In the reversal test the G_o/G_c values flagged with * indicate common K values, others not flagged have statistically different K-values for reverse and normal populations, in which case a simulation reversal test was performed. Plat and Plong are the latitude and longitude of the mean south virtual geomagnetic pole1. A95 (min, max) = Fisher 95% confidence interval for VGP-based site mean (Ns sites), and $A95_{min}$ and $A95_{max}$ threshold values of Deenen et al. (2014). Statistics determined with Pmagtool v.5 (Hounslow, 2023b). [a] = conventional Fisher mean using specimens. [b] = using method of McFadden and McElhinny (1988) to find great circle intersection points (T-class data) and combined with S-class line fits for each sample mean. [c] = great circle combined mean using the method of McFadden and McElhinny (1988) on specimen level data.

3. Results

3.1. Magnetic Mineralogy

Some 82% of the limestones have magnetic susceptibility <0 (Figure 4c), so they are diamagnetic. Positive susceptibilities are not particularly confined to any particular carbonate lithology other than the two rudstone samples. Instead, positive magnetic susceptibility is mostly related to more shaley and argillaceous stratigraphic intervals, such as the Woodbine Shale and those in the Alston Fm (Figure 4c). NRM intensity is largely independent of magnetic susceptibility, suggesting that these largely express different magnetic phases (Figure 4b).

Specimens show a large range in S-ratio and B_{cr}, indicating that there is a strong mixture between hard IRM behavior with B_{cr} >100 mT and soft behavior with S-ratio 0.4–0.8 (Figure 5a). The largest proportion of samples have S-ratio < −0.6 (histogram in Figure 5a) There is no strong correspondence with lithology, but rudstone (only 2 samples), mudstones, and argillaceous packstones have the larger positive S-ratios, and grainstones the smaller (i.e., negative) S-ratios on average (Figure 5a). Since pure hematite has B_{cr} typically 100–800 mT (Peters & Dekkers, 2003), and there is limited evidence in thermal demagnetization of goethite (but see Figure S5 in Supporting Information S1), the relationship in Figure 5a is inferred to reflect a variable magnetic mixture of hematite and a softer phase. Some 68% of specimens have B_{cr} >100 mT, which shows that samples are largely hematite dominated. Since only some 7% of the sample set can be directly associated with observed reddening at the emergent surfaces (Figure 4b), the hematite has been contributed to these limestones in other ways, in addition to directly at emergent surfaces. The HIRM and IRM_{40mT} are proxies for the total contributions from the hematite and soft component (Walden & White, 1997) and are weakly co-related (Pearson $R^2 = 0.41$, power-relationship in Figure 5b), indicating some connection between their supply. Samples associated with the emergent surfaces have variable but generally larger HIRM (Figure 5b), confirming the field data and petrographic observations of Horbury (1987) that the reddening at these surfaces is associated with hematite. Wright et al. (1997) have inferred

10.1029/2023GC011282

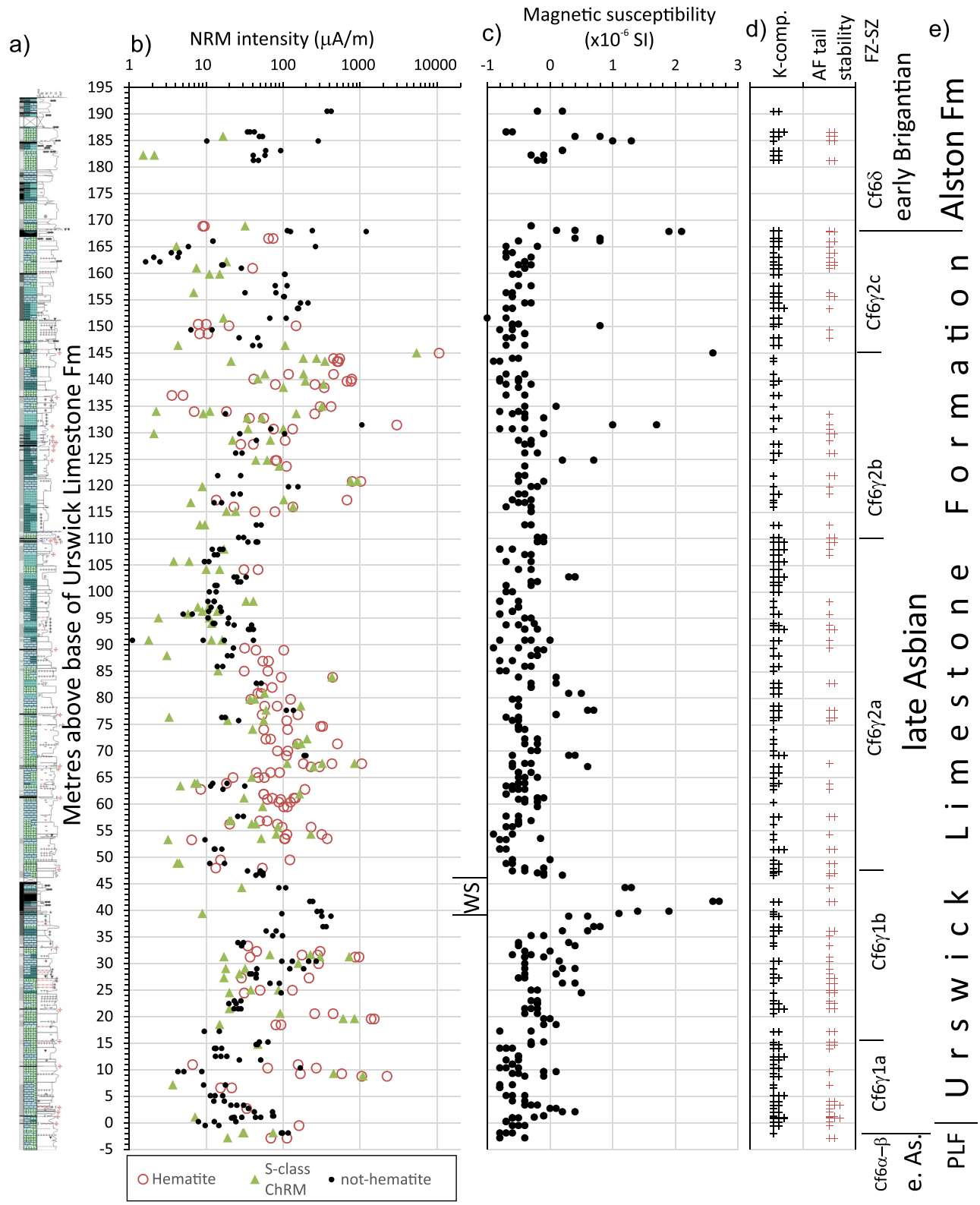

Figure 4. Specimen magnetic data for the Trowbarrow Quarry section. (a) shows a simplified log (sampling details in Figures S1–S3 in Supporting Information S1), and (e) shows the foraminiferal subzones and British substage boundaries (from Cózar et al., 2022b). In (b) the NRM intensities are partitioned into hematite and non-hematite magnetizations, and the ChRM intensity is also shown at the first demagnetization step at which the S-class ChRM is isolated. (d) The occurrence of the K-component and high stability tail during AF demagnetization. PLF = Park Limestone Formation, WS = Woodbine Shale, e.As = early Asbian. FZ-SZ = foraminiferal zone and subzone.

one hypothesis, namely that this may come about by "terra-rossa- type" insoluble residuals during karst formation, although evidence for this is sparse (Hounslow, Cózar, et al., 2024).

The Silverdale-Arnside area around Trowbarrow is not impacted by the hematite-mineralization like that seen in the Furness Peninsula in southwest Cumbria (Rose & Dunham, 1977; Figure 2). However, trace amounts of hematite mineralization do occur in the nearby area as: (a) micron-scale coatings along some joint surfaces (probably mostly from Holocene karstification, since it is a near-soil-surface feature). This is fairly sporadic in its distribution, but occurs in parts of the Park Limestone at Trowbarrow in those parts of the sections below that sampled. Since Trowbarrow is a deep quarry, this is not seen in the sampled parts of the faces; (b) Rarer mm-sized pods and veins of hematite, which can be associated with dolomite veining, are sometimes seen to amalgamate and grow from joints. This type of veining seems to be younger than the more common white ferroan-calcite calcite veining described by Horbury (1987). This dolomite-hematite veining is common in sections in the Furness Peninsula (localities 1, 2; Figure 2) but has not been seen in the Trowbarrow samples; (c) More substantive hematite mineralization in fault networks and calcite-dolomite-filled fracturing/faulting. Sections at Trowbarrow are not affected by this to any extent. Hence, these macroscopic forms of hematite mineralization are unimportant in the Trowbarrow samples. Also, the rare partial dolomitization in thin sections concurs with the largely primary nature of the carbonates.

The soft magnetic component appears to be in part associated with argillaceous material, with the median IRM_{40mT} being larger in the argillaceous wackestones and packstones (Figure 5b). Since hematite does not significantly acquire ARM (Peters & Thompson, 1998), this measurement provides a window into characterizing the soft component in these mixed-mineralogy samples. $\%d.ARM_{40mT}$ is typically 30%–40%, as seen in harder magnetites found in deep-sea sediments, older sediments and reference rocks (Figure 6a). These are unlike the soft ($\%d.ARM_{40mT}$ <20%) ARM behavior seen in multi-domain (MD) pyrrhotite (Figure 6a) or in MD titanomagnetite, as seen in less-oxidized basalts (Figures 6a and 6b). Unoxidized titanomagnetites are fairly uncommon in sediments due to pre-sedimentation oxidation and diagenetic modifications (Roberts, 2015) and seem unlikely in these limestones deposited under oxidizing conditions. Likewise, greigite and hard pyrrhotite have $\%d.ARM_{40mT}$ larger than 45% (Hounslow et al., 2023; Peters & Thompson, 1998), indicating that these phases do not occur in significant proportions in the Trowbarrow limestones. Therefore, the soft behavior in these samples is either due to magnetite or an intermediate stability pyrrhotite (<20 μm in grain size; Figure 6b). McCabe and Channell (1994) also detected no pyrrhotite low temperature transition in their Craven Basin samples.

The ratio of saturation IRM and χ_{ARM} is indicative of particle size and interaction in low Ti magnetites (Moskowitz et al., 1993; Oldfield, 1999; Peters & Dekkers, 2003). However, because of the additional presence of hematite in the Urswick Limestone Fm, we use the IRM_{40mT}/χ_{ARM} as a comparable proxy and compare this to available reference materials (Figure 6b). The bulk of the Urswick Limestone Fm samples fall at the lower IRM_{40mT}/χ_{ARM} end of the natural magnetite and Indian Ocean reference magnetite materials. Reference material of intermediate and high stability pyrrhotite likely has IRM_{40mT}/χ_{ARM} > 2 k A/m between the synthetic pyrrhotite and natural detrital pyrrhotite <20 μm in size (Figure 6b), perhaps similar to four samples from Trowbarrow.

The few successful samples measured for RRM indicate small positive and negative Bg values, and ARM_{ROT}/ARM less than 0.6 (Figure 6c). These are similar to reference materials of magnetite-bearing siliciclastics and magnetofossil-bearing chalks (Hounslow et al., 2023). The Trowbarrow data indicate distinctively different RRM behavior to the Taiwanese pyrrhotite (ARM_{ROT}/ARM >1.2), and the Taiwanese greigite with Bg < −10 μT. However, the unusual behavior of the Urswick Limestone Fm samples is the dominance of specimens with Bg > 0, which was restricted to only a few magnetite-bearing samples tested by Hounslow et al. (2023). This may be because of the incompletely known range in Bg for natural magnetite under the test conditions. One sample was also tested for variation with rotation rate, which did not change this conclusion (Figure S6 in Supporting Information S1). The two specimens from the additional set tested with low temperature measurements suggest a weak Verwey transition indicative of some unoxidized magnetite (Figure S5 in Supporting Information S1).

In summary, the magnetic mineralogy in the Urswick Limestone Fm is dominated by hematite, with a variable contribution probably from fine-grained non-interacting magnetite, which is probably detrital in origin. The hematite is Carboniferous in age and likely deposited with the carbonates, but in a small number of cases may be generated via emergent surface formation (Hounslow, Cózar, et al., 2024). Based on correspondence with carbonate cycles at Trowbarrow, and a feasible environmental model of the non-carbonate inputs, the bulk of the hematite was likely delivered as eolian dust from far-field sources (Hounslow, Cózar, et al., 2024). There is a

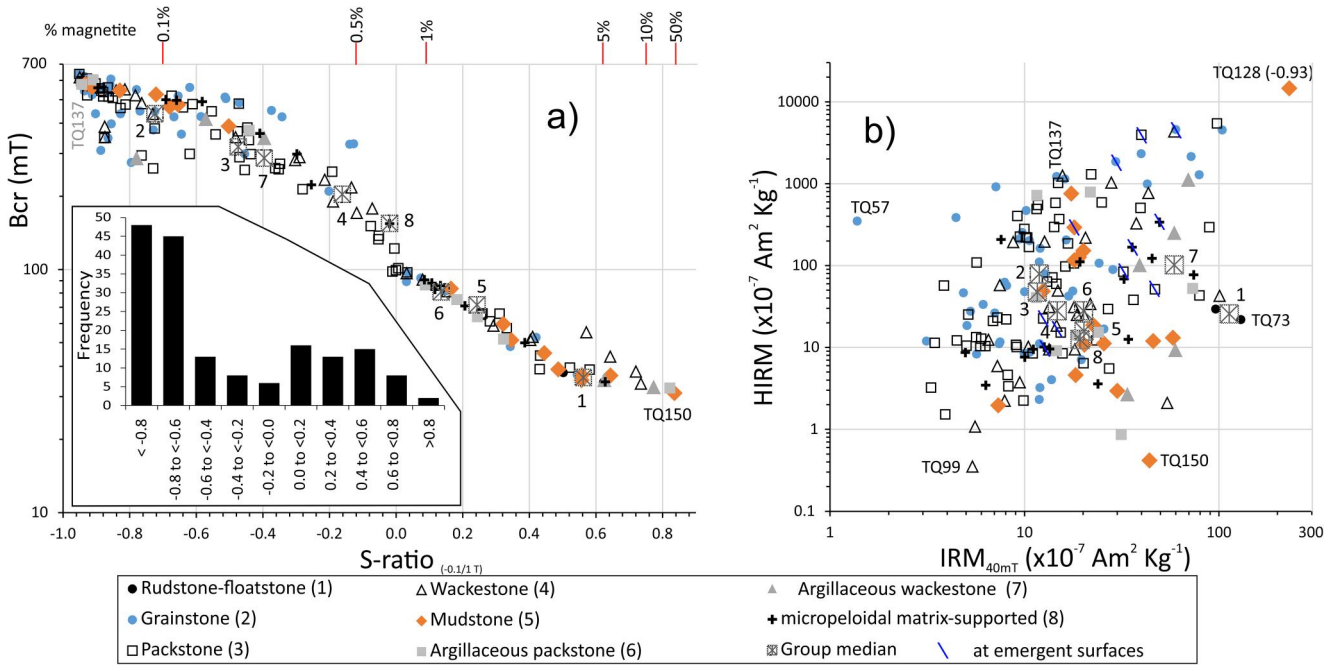

Figure 5. Isothermal remanent magnetization (IRM) data for samples from Trowbarrow Quarry, segmented according to the petrographic data in Cózar et al. (2022b). Key applies to both (a) and (b). The %magnetite scale on the top of (a) is based on the hematite-magnetite mixing relationships of Frank and Nowaczyk (2008) applied to the S-ratio (-IRM$_{0.1mT}$/1T). The medians of the petrographic groups are indicated with a crossed-square and labeled with group numbers 1 to 8 (as in key). Specimen corresponding to extremes in the S-ratio (in a) and extremes in (b) are indicated.

speculative possibility that the soft component may in part be of magnetofossil origin (i.e., with low ARM$_{ROT}$/ARM; Figure 6c). Approximate estimates of the relative mass contribution to the IRM can be obtained using the hematite-magnetite mixing experiments of Frank and Nowaczyk (2008) (see scale on upper Figure 5a). A detrital origin of magnetite for Asbian limestones from the Craven Basin was demonstrated by Turner (1975). Their optically observable magnetite was intimately associated with ilmenite and hematite and had B$_{cr}$ of 33–37 mT and showed the Verwey transition. Pyritization of these was also typical. The same may apply to the soft phase here, since pyrite is common in the Urswick Limestone Fm (Horbury, 1987). The additional set likely has a mineralogy similar to those at Trowbarrow.

3.2. Paleomagnetic Results

The response of the specimens to demagnetization depended on their magnetic mineralogy. For those that were dominated by hematite, thermal demagnetization was used up to about 650–700°C. For those not dominated by hematite, a combination of thermal demagnetization from 250 to 450°C (300°C most commonly) followed by AF demagnetization worked best, since this allowed better isolation of the small ChRM (see Figure S9 in Supporting Information S1 for demagnetization diagrams). Thermal demagnetization alone on these types of samples often obscured the ChRM. This was the prime reason Palmer (1987) failed to identify any primary magnetization in Visean limestones from this region. The alteration crisis identified by the susceptibility measurements was commonly around 350°C, but lower (~200–250°C) in darker wackestones, and up to 400–500°C in some more thermally stable grainstones.

3.2.1. Trowbarrow Quarry Set

The specimens generally displayed three components, first a low stability (LT) component was generally removed by ~180–200°C with some larger unblocking temperatures for a few samples (Figure 7a). Some 80% of specimens contained this component. Second, an intermediate stability component (K-component) was often the strongest component present, displaying southerly directed magnetization of shallow inclination (~±10°) in stratigraphic coordinates and mostly negative inclinations in geographic coordinates (Figure 7b). In the 66% of specimens in which hematite dominated the magnetization, the K-component was weaker or absent. Some 62% of

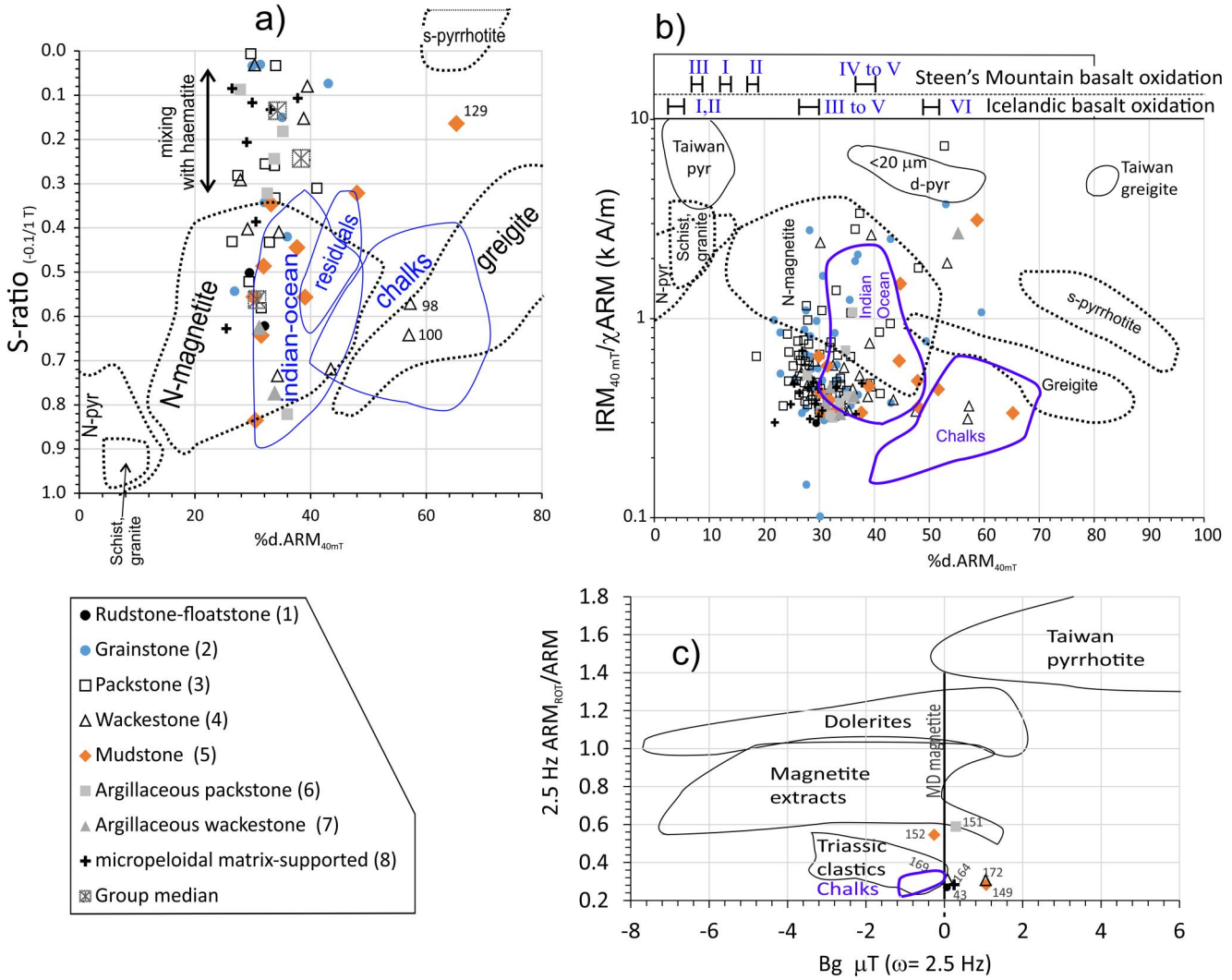

Figure 6. (a), (b) IRM and anhysteretic remanent magnetization (ARM) data, and (c) rotational remanent magnetization (RRM) data used for characterizing the soft magnetization. Data points use the key shown with sub-sets of the specimens in (a) and (c) and all the specimen data in (b). The various "envelopes" represent well characterized reference magnetic materials as used by Peters (1995), Peters and Thompson (1998) and Hounslow et al. (2023). Top of (b) shows the range of %d. ARM_{40mT} from Dunlop (1983) for basalts with well-defined titanomagnetite oxidation status. These reference data are listed in Table S4 in Supporting Information S1. Reference data from Peters (1995) are: N-pyr = 8 natural pyrrhotites, S-pyr = two synthetic pyrrhotites; Schist, granite = three magnetite-bearing schist and granodiorite samples; N-mag = 15 igneous rock and peat samples with magnetite as dominant phase; greigite = 14 natural SD greigite samples (North Sea cores). Reference data from Hounslow et al. (2023): Indian Ocean = 12 biogenic carbonates with eolian-clastic magnetite and some magnetite magnetosomes. Residuals = 4 samples of residual (after extensive diagenesis) magnetite and ferrian chromite dominated magnetic phases. Chalks = 12 samples of coccolith chalks, with soft magnetization dominated by magnetite magnetosomes. Taiwan pyrrhotite = 5 samples of sized modern detrital monoclinic pyrrhotite (<20 µm data in (b) and 4 monoclinic pyrrhotite-bearing schists (plus sized >20 µm data in b as "Taiwan"). Taiwan greigite = 4 samples of SD greigite. In (c) only: Dolerites = 3 samples of Svalbard dolerite; magnetic extracts = 16 magnetite-dominated extracts corresponding to Indian Ocean and residual-magnetic phases in (a) and (b); Triassic clastics: 30 samples of Late Triassic marine and non-marine sandstones and siltstones from Svalbard.

all specimens displayed the K-component clearly enough for a PCA line fit. Third, a dual polarity ChRM (Figure 8a) was usually the highest stability component. Some 34% of all specimens displayed a component suitable for a PCA line fit (i.e., S-class data), with the remainder (55% of specimens of T-class) displaying this component as great circle trends toward the ChRM directions (Figure 8b). The strength of the S-class ChRM component is largely related to the initial NRM intensity (Figure 3b), although in many non-hematite- dominated specimens the initial appearance of the ChRM was typically below an intensity of 100 µA/m.

The LT component is typically quite small in intensity, and most often shows a very well-defined break on Zijderveld diagrams from the intermediate stability K-component. The LT component has a fair scatter, with a

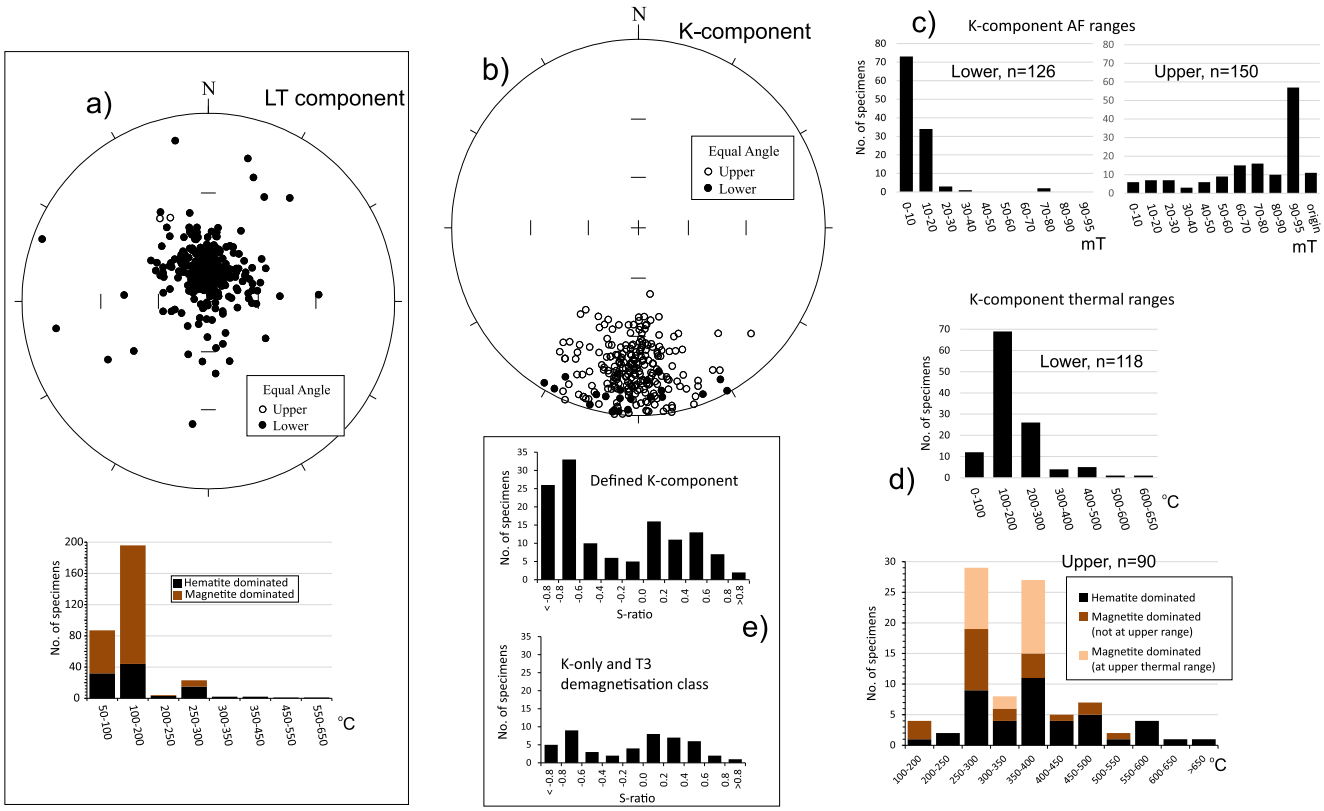

Figure 7. Directional and unblocking data for the low temperature LT and K-components from Trowbarrow Quarry specimens (in geographic coordinates). (a) the LT component and its upper unblocking temperature for magnetite (mean ~180°C) and hematite-dominated (mean ~ 200°C) magnetizations, (b) the K-component directions. (c) K-component alternating field (AF) ranges and (d) lower and upper thermal demagnetization ranges, with the upper-range set partitioned into dominant type of magnetization, and for the combined demagnetization scheme, if this temperature matches the uppermost thermal step. These data also include composite thermal-AF ranges (24 specimens); n = amount of data in each graph. (e) The S-ratio of those samples in which the K-component is defined (upper) and in which the magnetization are T3 class or contain no ChRM and are entirely dominated by the K-component (bottom). Directional data for additional sample set in Figure S9 in Supporting Information S1.

mean direction (geographic coordinates) of 356, +73, $\alpha_{95} = 2.2$, $k = 14$, $n = 316$ (Figure 7a). This is interpreted as primarily a Brunhes-age component (geocentric axial dipole inclination at site = 70°). A very similarly behaved Brunhes-age component was reported by McCabe and Channell (1994) from the Craven Basin.

The intermediate stability K-component is evenly distributed throughout the section (Figure 4d) and this dominates in 4.3% of specimens to the extent that no ChRM could be detected. Using thermal demagnetization, the K-component was most often seen between 200 and 400°C, but lower and higher unblocking ranges were also seen (Figure 7d). The upper temperature range of the K-component is around 300–400°C with the median for hematite dominated magnetization at ~400°C and for magnetite-dominated magnetization ~300°C. McCabe and Channell (1994) report a similar typical 200–450°C unblocking range for their inferred Kiaman-age component from the Craven Basin limestones. For those subjected to the composite demagnetization scheme, the K-component is most commonly seen from the 5–20 mT steps until AF steps to 60 mT or higher. However, the upper AF step that removes the K-component has a wide range in the AF field (Figure 7c). The K-component does not have a strong bias with S-ratio, having a distribution similar to the overall sample set (Figures 7e and 5a). This suggests that it is carried by both hematite and magnetite. The K-component has a mean direction (in geographic coordinates) of 182.3°, −14.4°, $\alpha_{95} = 1.9°$ ($k = 24.3$, $n = 244$; VGP = −43.1°, 354.4°; Figure 7b) and is interpreted as a Kiaman-age partial remagnetization, similar to that widely reported from other Visean limestones and pre-Carboniferous rocks in Britain (Channell et al., 1992; Palmer, 1987; Piper & Crowley, 1999; Setiabudidaya et al., 1994). The paleopole derived from this mean is similar to those from other Kiaman remagnetizations elsewhere in Europe (Figure 9), which are mostly a little to the east of the stable Europe apparent polar wander path of Torsvik et al. (2012).

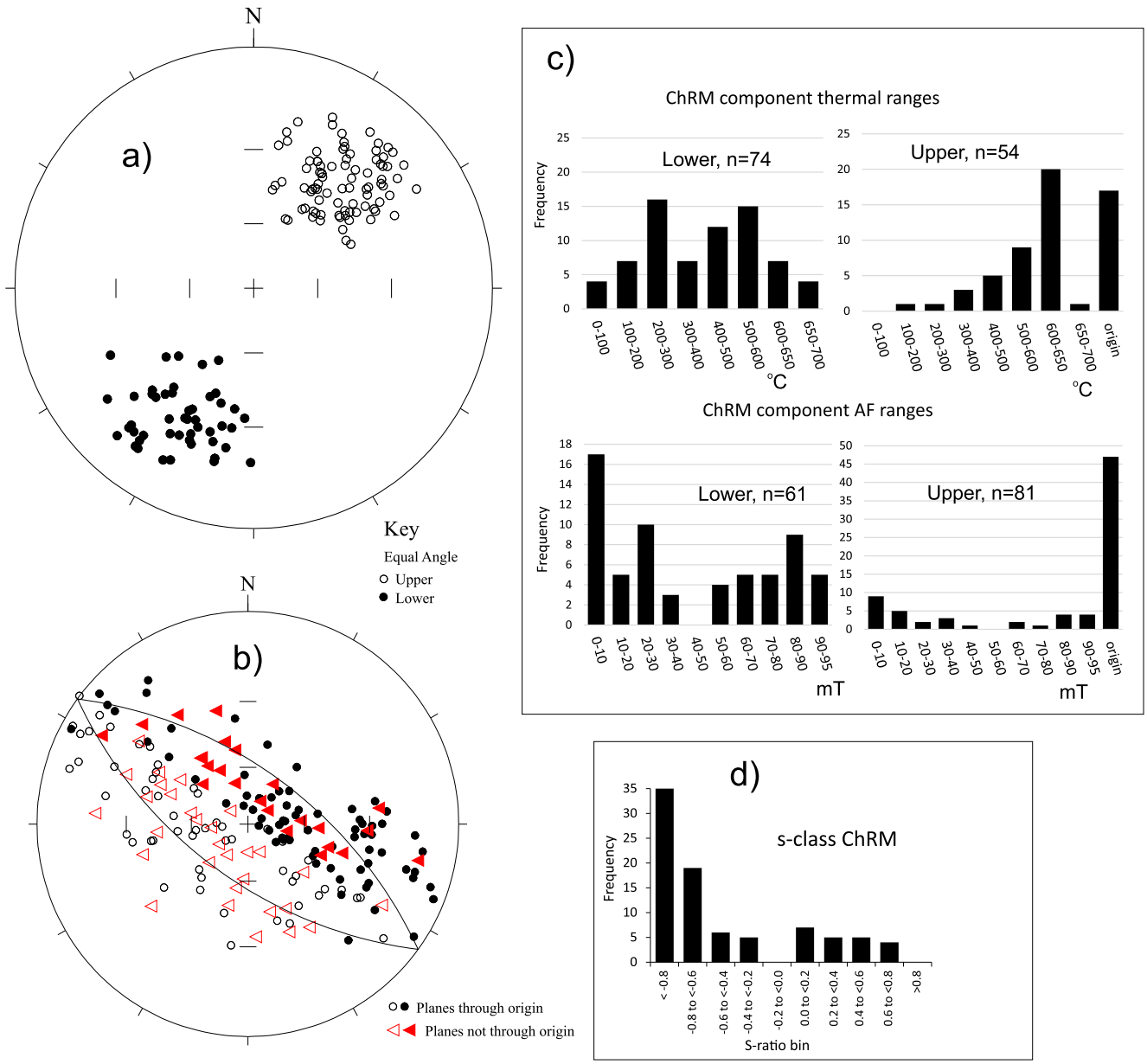

Figure 8. Directional data for the ChRM component, with line fits (S-class data) in (a) and poles to the fitted great circles in (b). The single great circle plane in (b) is that normal to the mean of the S-class data. (c) S-class ChRM lower and upper thermal demagnetization ranges (in upper bar graphs) and alternating field (AF) ranges (in lower bar graphs). These data also include composite thermal-AF ranges (20 specimens); n = amount of data in each graph. (d) The S-ratio of those specimens which have an S-class ChRM.

The dual polarity ChRM is nearly always the highest stability component (Figure 8c) seen in thermal demagnetization. In geographic coordinates, this dual polarity direction has an axis at ~026° with inclination of ~35°. The ChRM is commonly observed going to the Zijderveld origin, particularly so for isolation using AF demagnetization (Figure 8c). Thermal alteration at >600°C may obscure origin fits, so end-ranges in this case are more commonly 500–650°C (Figure 8c). The line-fit (S-class) ChRM data is somewhat biased toward the most negative S-ratios (Figure 8d). A subset of 7 specimens shows S-class line fits for the ChRM prior to isolation of the K-component. Some 39% of specimens show no clear K-component but have the ChRM in the mid stability range (i.e., thermal upper range 200–400°C and AF upper range <40 mT; Figure 8c). This somewhat unpredictable overlap in the stability range of the K-component and the ChRM is likely responsible for the large number of specimens with great circle type behavior. Notably, those few showing only the K-component (4.3% of

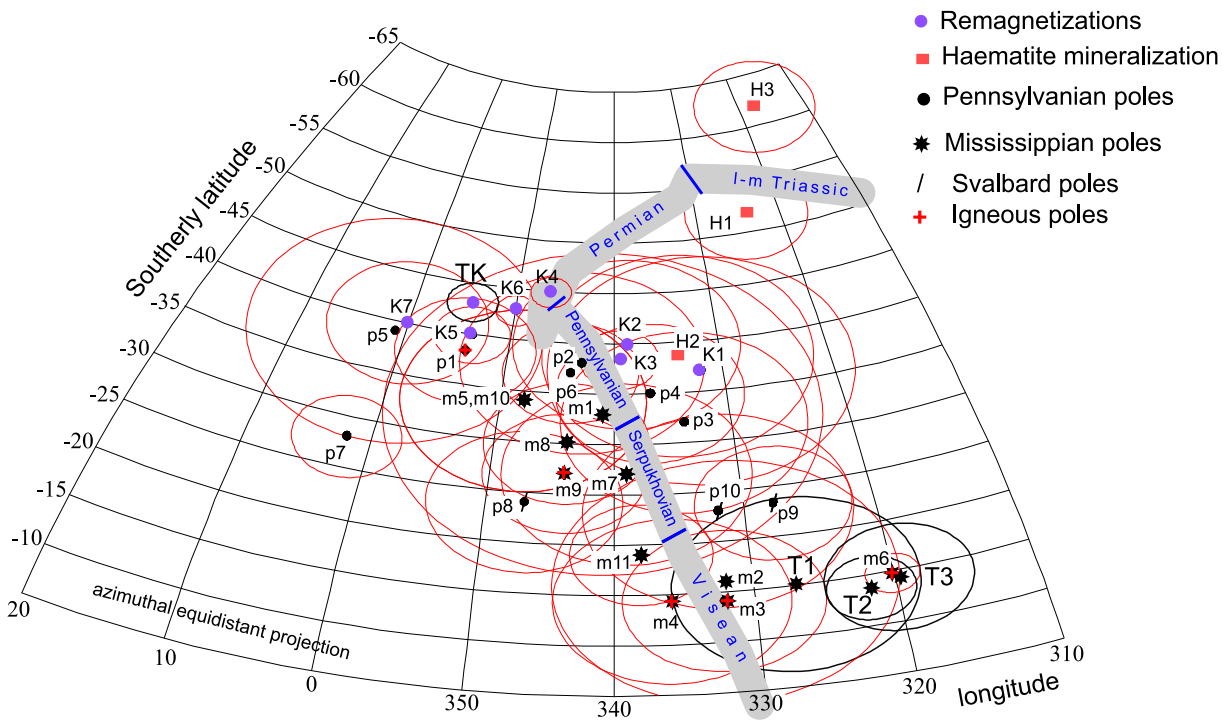

Figure 9. South paleomagnetic poles for the three S-class means (and their A_{95} confidence cones) from Trowbarrow Quarry (T1, T2, T3) and that of the K-component from Trowbarrow (TK) placed alongside the stable Europe apparent polar wander path of Torsvik et al. (2012) partitioned into age intervals (using their timescale). Other paleopoles are selected Mississippian (m1 to m11) and Pennsylvanian (p1 to p7) poles and inferred Kiaman-age reverse remagnetizations (k1 to k7). Also shown are the paleopoles of the Cumbrian and Isle of Man hematite mineralization's (H1 to H3) of Rowe et al. (1998) and Crowley et al. (2014). Inverted azimuthal equidistant projection. See Table S5 in Supporting Information S1 for sources of other data in this figure.

total) or the T3 class of great circle trends (17.1% of total) tend to be biased toward the magnetically softer-end (most positive) of the S-ratio classes (Figure 7e). For a normal polarity ChRM, this stability overlap is characteristically expressed as a great circle trend toward the NE, and sometimes an increase in intensity, as the approximately opposite K-component is removed. A particular feature of some specimens subjected to combined AF demagnetization is a high stability tail (Figure 3d), in which an AF-resistant phase (i.e., hematite) is evidently carrying the ChRM but cannot be fully demagnetized with the composite scheme. This behavior also contributes to the dominance of the great-circle type behavior.

The Trowbarrow data has been divided into three stratigraphic intervals for the purpose of defining directional sets to be used in the fold test of the ChRM (Table 1) and two sets for fold tests on the K-component (Table 2). This was to enable rather closer sample-group sizes for the fold test and parametric bootstrap-based estimates of the likely unfolding percentage. The whole-section mean is probably more applicable to a paleopole estimate (Table 1).

Fisher mean directions using the S-class data generally fail the reversal tests, with inverted dual polarity directions ~10° different. Nevertheless, the mean VGP, A95, is within the thresholds of Deenen et al. (2014), indicating that dispersion is within the expected secular variation range (Table 1), and the dispersion (precision parameter *k*) is similar in the dual polarity sets (Figure 8a). The reversal test failure could be due to a small fraction of the K-component remaining in the ChRM directions (see Section 3.3). A combined great circle mean (method of McFadden & McElhinny, 1988) was also determined for the three intervals independently (Table S3 in Supporting Information S1). For the T-class specimen data, the directions from this were used to define site (i.e., sample) means, since generally, 2–3 specimens were measured from each sample. This mean displays similar but slightly shallower mean directions than the S-class means (Table 1, Table S3 in Supporting Information S1) and is closer to antipodal. The paleopoles derived from the S-class directions (and site means) are similar to other Visean volcanic poles from stable Europe (Figure 9), supporting the reliability of the directional analysis.

Table 2
Mean ChRM and K-Component Directions From the Additional Localities

Locality and groups	Dec(°)	Inc(°)	K/α_{95}(°)	Ns/Nl/Np
ChRM means				
11–13 (RD) [a]	208	16	14/15	7/2/7
14 (MG) [a]	205	37	34/10	5/4/4
5,4,7 (GK1-GK7) [a]	211	35	11/15	8/2/9
6,2 (GK8-10, DF1-3) [a]	219	32	20/12	4/5/4
8 (GK11-13) [a]	233	48	7/32	3/1/5
9 (AS5-AS8) [a]	234	27	20/16	4/3/3
K-component means				
6, 8 (GK2)	183	−16	16/13	6/9/0
11–14 (RD-MG)	211	−27	38/15	3/4/0
3, 4,5,7,10 (GK1)	187	−16	21/7	11/23/0
9 (AS)	191	−15	62/6	4/5/0
2 (DFa)	180	7	65/10	2/5/0
1 (DFb)	198	−34	45/8	4/8/0
TQ1	182	−16	23/3.8	58/116/0
TQ2	183	−13	26/2.5	64/128/0

Note. ChRM in stratigraphic coordinates. K-component in geographic coordinates. TQ1 and TQ2 sets are the Trowbarrow Quarry dataset partitioned into a near vertical set (mean dip direction = 269.5°, 86.2°), and a less steeply overturned set (mean dip direction = 268.5°, 80.2°). Codes in () are the sampling codes indicated in Table S1 in Supporting Information S1. [a] = great circle combined mean using method of McFadden & McElhinny (1988) on specimen level data.

3.2.2. The Additional Sample Set

Demagnetization behavior of the additional set was similar to that from Trowbarrow Quarry (Figures S7, S10 in Supporting Information S1). In these also, both the LT and K-components were present alongside a dual polarity ChRM, which in most cases, was only a small fraction of the initial remanence (Figure S10 in Supporting Information S1 shows demagnetization diagrams). The remanence intensity was similarly often dominated by the K-component. Of the 103 specimens measured (42 samples), 51% displayed evidence of a Carboniferous magnetization (17% S-class; 34% T-class specimen data). When grouped by localities, the ChRM mean directions are similar to those at Trowbarrow (Table 2; Table S3 in Supporting Information S1). Of these specimens, 47% were reverse polarity and 53% were normal polarity.

Some 25% of specimens displayed only evidence of the LT component or the K-component (9% and 16% respectively) without any evident ChRM. These overprints were scattered throughout the localities but were dominant at localities 1 and 10. The remaining 22% of specimens were strongly impacted by strong thermal alteration during thermal demagnetization or erratic directional behavior. The mean direction (in geographic coordinates) of the LT component is 351°/+75° ($n = 71$, $k = 11.6$, $\alpha_{95} = 5.2°$), much like that seen at Trowbarrow.

These additional localities give a (sample) mean K-component direction (without locality 2) of 190°/−20° ($\alpha_{95} = 3.9°$, $k = 16$, $n_{localities} = 5$) some 9° different from that seen at Trowbarrow (Table 2; Figure S11b in Supporting Information S1), which is significant using the test of McFadden and McElhinny (1990). In addition, the sample-based means of the K-component show a fair degree of dispersion (Table 2; Figure S11c in Supporting Information S1), which together could suggest some post-Permian tilting or rotation. However, fold tests on the K-component indicate that this component was acquired close to zero percent untilting (Table 3), with 95% confidence limits on tilting, which include zero untilting (Figures S14 and S15 in Supporting Information S1). The Fisher block rotation fold test of Enkin and Watson (1996), which accounts for vertical axis rotations, gives better grouping at zero untilting.

Fold tests were performed using ChRM directions recovered from the additional and Trowbarrow sets combined. These used different data groupings to the K-fold test, since; (a) ChRM and K-components were not evenly distributed across the localities, (b) bedding dips varied at most localities, and (*c*) the requirements of the parametric bootstraps on the fold tests require minimum numbers of data. Consequently, some localities were regrouped. The fold tests support the conclusion that the ChRM was acquired pre-tilting (Table 3; Figures S12 and S13 in Supporting Information S1). The rocks from locality 14 are notably younger than the remaining, largely Visean localities, but excluding this locality does not significantly impact the fold test. A fold-test was not possible using only the Trowbarrow dataset, since bedding dip dispersion is too small.

3.3. Magnetostratigraphy at Trowbarrow

The section is dominated by normal polarity with the 182 sampling levels comprising 76.4% normal, 20.9% reverse and 2.8% of unknown polarity (Figure 10). The inferred polarity quality is generally unevenly distributed with demagnetization behavior with N, R and R? groups containing the bulk of the S-class behaviors, and the other groups the bulk of the T-class data (Figure 3b). Conversely, the VGP_R latitudes are only weakly related to the polarity quality groups (Figures 3c and 3d) due to their dependence on angular dispersion from the mean pole, something which is more weakly represented in the qualitative polarity quality groups. The VGP_R latitudes have a similar dispersion between normal and reverse polarity (Figures 3c and 3d; 10) suggesting that any possible directional contamination is equally represented in both polarities.

Table 3
Fold Tests on the ChRM and K-Components

Fold test type and locality	Sets	Bootstrap type	%U [−/+] or %U {p_0, p_{100},%s}	Ng/N	Figures in Supporting Information S1
ChRM means					
TQ + additional (no 2, 14)					
Progressive unfolding	grouped	parametric	106 [101,113]	8/-	S13a
TQ + additional (no 2)					
Progressive unfolding	grouped	parametric	108 [102,112]	7/-	S13b
McFadden	grouped	none	100 {0, 0.8, none}	7/-	
additional (no 2, 14)					
Progressive unfolding	grouped	parametric	112 [97,127]	5/-	S13c
additional (no 2)					
Progressive unfolding	grouped	parametric	111 [96,127]	6/-	S13d
McFadden	grouped	none	100 {0, 2.4, none}	5/-	
K-component tests (all rows in Table 2)					
Progressive unfolding	specimens	Re-sampling	4 [−7/+15]	-/303	S15a
Progressive unfolding	grouped	Parametric	5 [−2/+13]	8/-	S15b
Fisher block rotation	grouped	Parametric	0 [−10/+10]	8/-	S15c
McFadden	grouped	none	15 {0%, 0%; none}	8/-	
Excluding site 2					
Progressive unfolding	specimens	Re-sampling	1.7 [−5.7, 9.7]	-/298	S15d
Progressive unfolding	grouped	Parametric	−5 [−15,5]	7/-	S15e
Fisher block rotation	grouped	Parametric	0 [−10/+10]	7/-	S15f
McFadden	grouped	none	5 {0%, 0%; none}	7/-	

Note. Set is using either the specimen-data or grouped data (partitioned by bedding dips) as in Table 2. %U = most-likely unfolding percent and 95% confidence limits on unfolding displayed in [−/+.]. p_0, p_{100} are the probability of exceeding the f-statistic for the 0% and 100% unfolding cases respectively, that is, values <5% indicate the 0% or 100% unfolding scenarios are unlikely. *%s* = the acceptable unfolding percent for a synfolding solution. 95% confidence limits determined with 1,000 bootstrap simulations. Ng = number of site groups (with similar dips), *N* = number of specimens. The ChRM data from Trowbarrow (TQ site) was grouped into three sets, the Lower Urswick Limestone Fm, Upper Urswick Limestone Fm and the Humphrey Head Mb + Alston Fm. For the ChRM tests locality 2 was not used in the McFadden (1998) fold test since it has too few points. Using Pmagtool v.5 (Hounslow, 2023b). The DC foldtest of Enkin (2003) cannot be easily applied here since the bedding dips vary in the groups. Progressive unfolding is the test of Watson and Enkin (1993), and Fisher block rotation that of Enkin and Watson (1996).

Nine reverse magnetozones (TQ0r to TQ5r.1r, TQ5r.2r to TQ8r) are defined with two or more adjacent samples, each with multiple specimens (Figure 10e). Seven sub-magnetozones (TQ2n.2r, TQ4n.1r, TQ5n.1r, TQ5r.1n, TQ7n.1r, TQ7n.2r and TQ9n.1r) are defined with multiple specimens from a single sample. Two rather more tentative submagnetozones are defined with one or two lower quality specimens (TQ2n.1r, TQ9n.2r; Figure 10e).

Cózar et al. (2022c) have proposed a set of regionally correlated (between Ireland, northern England and south Wales) emergent surfaces, with Trowbarrow as the reference section (Figure 10a). Independent means of assessing the missing time in the rock record at these emergent surfaces could be based on a variety of generalized modeling and observational data (Barnett et al., 2002; Rygel et al., 2008), and cyclostratigraphy (Hounslow, Cózar, et al., 2024). If the magnetic polarity changes across the emergent surface, this suggests a possible missing interval, since there is no reason to suppose that changes in polarity and drops in sea-level should be coincident (unless by chance). Four of the emergent surfaces (O'a, II, Iva and XII) display a switch in polarity across these surfaces, suggesting that missing intervals may be present at the bases of magnetozone TQ2n, TQ2n.2n, TQ4n.1r, and TQ9n.2n. Also, the complex of paleosols around emergent surface X, show a change in polarity across the overlying paleosol at 129.5 m (base of TQ7n.2r). Other emergent surfaces do not coincide with polarity changes, so polarity offers no evidence of likely missing intervals. The base of TQ8n occurs some 1.5 m above surface XI, possibly coincident with a prominent burrowed surface some 70 cm below sample TQ142. Emergent surface VII is the most intensely mamillated surface and has the thickest silty paleosol in the quarry; therefore, it may

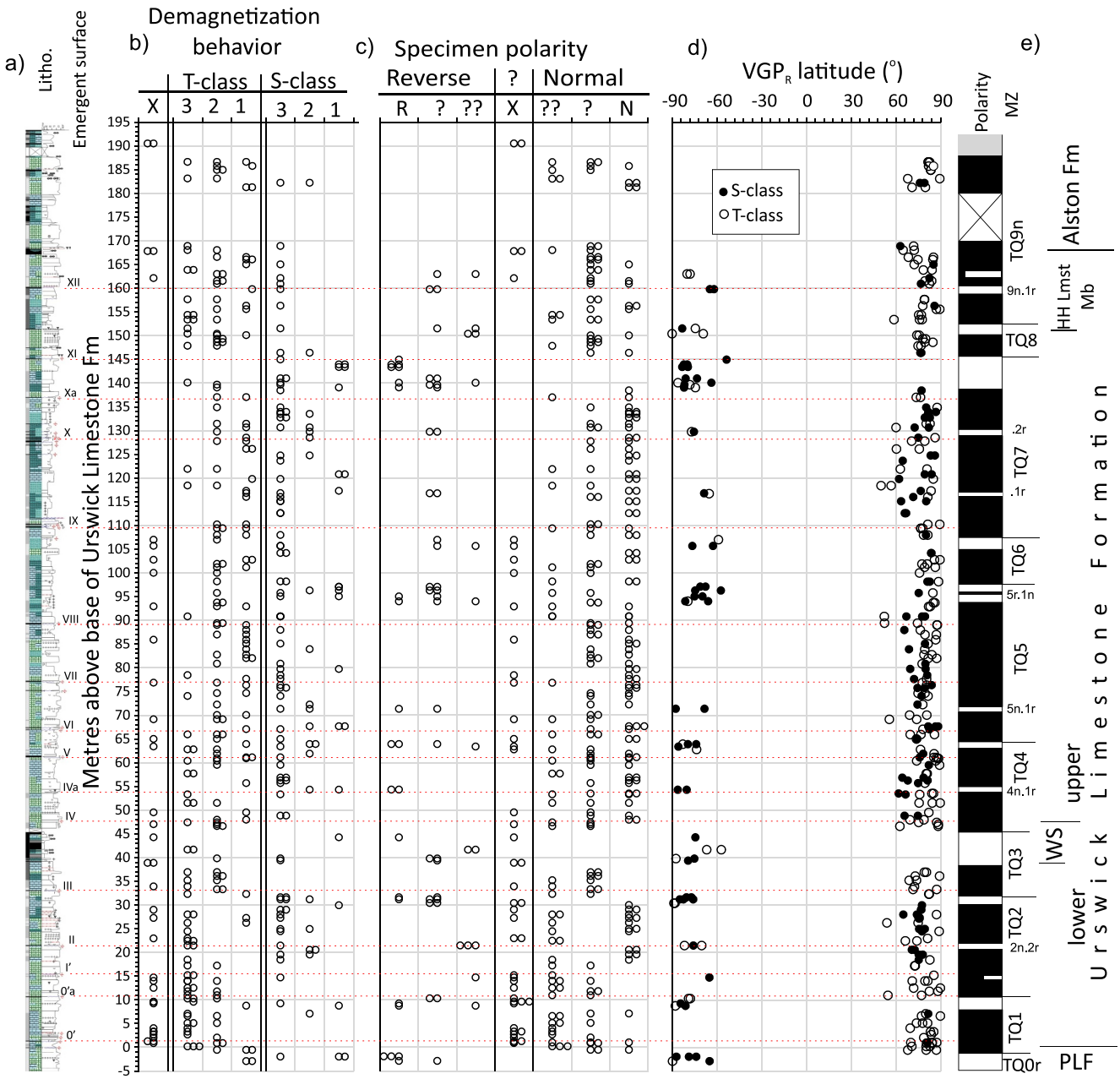

Figure 10. Magnetic polarity data from Trowbarrow Quarry. (a) a simplified lithologic log (sampling details in Figures S2 and S3 in Supporting Information S1), with major emergent surfaces (O' to XII) of Cózar et al. (2022c), (b) specimen demagnetization behavior, (c) inferred specimen polarity, (d) VGP$_R$ latitude and (e) geomagnetic polarity, with numbered magnetozones (MZ). PLF = Park Limestone Fm. WS = Woodbine Shale, HH Lmst Mb = Humphrey Head Limestone Member.

represent the longest hiatus using the criteria of Wright (1994), although the polarity does not change at it. Sedimentation rate models for the section based on cyclostratigraphy suggest that surfaces II, VI and VII are the most important hiatuses in the section (Hounslow, Cózar, et al., 2024) with missing intervals of ~30 ka, ~50 ka and ~19 ka, respectively. However, the eccentricity-modulated cyclostratigraphy is unable to reliably detect hiatuses <~10 ka. Hence, of these three, only surface II could be indicative of a more substantial truncation of TQ2n.2n or TQ2n.2r (Figure 10e).

4. Discussion

4.1. The Origin of the K-Component

Fold tests on the K-component suggest that it was acquired close to zero untilting. This test is principally one using the steeper bedding dips (associated with the Silverdale monocline at Trowbarrow and locality 9) compared to the less steeply dipping strata in other sections. However, there are several potential phases of tilting in this region. These are principally related to Late Pennsylvanian-Early Permian basin inversion, and later extension-related tilting in the Permo-Triassic, associated with the formation of the Irish Sea Basin and the Craven Fault systems (Kirby et al., 2000). If the K-component was acquired before the Permian-Triassic, it is possible Permian-Triassic tilting introduced some additional dispersion in the K-component locality means. Any Permo-Triassic tilting has the most impact at localities 1 and 2, since these occur in the Furness Peninsula, which is more severely affected by the boundary faults of the Irish Sea Basin (Kirby et al., 2000). In the Craven Basin, fold tests of the K-component are principally associated with datasets from the Clitheroe anticline (McCabe & Channell, 1994) and the Skipton anticline (Palmer, 1987; dataset reworked here), with both indicating that the K-component was acquired synfolding (at 63% and 50 ± 17% unfolding, respectively). Since both these anticlinal structures are Variscan in origin (Kirby et al., 2000), it seems unlikely that Permo-Triassic extensional faulting in the Craven Basin added further additional tilting to these structures.

To examine the mineralogical origin of the K-component, NRM intensity and rock magnetic datasets were partitioned into specimen sets which contained no K-component, contained a ChRM and the K-component and contained only the K-component (Figure 11). Many proposed remagnetization mechanisms involve introduction of new magnetic phases (Elmore et al., 2012), which should give enhanced NRM intensity and magnetic mineral abundance proxies for specimens with remagnetizations. For the Trowbarrow specimens the NRM intensity for those containing the K-component is not enhanced over those without (Figure 11a), although the intensity from magnetite-dominated samples is rather more focused around 10–60 μA/m and 100–400 μA/m, with the highest intensity specimens more represented in the group without the K-component. The χ_{ARM} shows similar relationships, with more of a bias toward middling to large χ_{ARM} for those specimens containing the K-component (Figure 11b). Significantly, the K component is present in both magnetite- and hematite-dominated magnetization (Figure 11a). These relationships which would tend to favor a thermoviscous (TVRM) origin (Kent, 1985; Dunlop et al., 1997) of the K-component (and LT component, Figure S16 in Supporting Information S1). However, it is conceivable that remagnetization could result from replacement or transformation of existing particles without modifying the Fe-oxide abundance. Processes such as annealing of vacancies (in hematite or magnetite) or magnetite to maghemite oxidation during prolonger burial at low temperatures could conceivably produce burial-related magnetization. For those containing the K-component, IRM_{40mT}/χ_{ARM} values are more focused within the mid part of the range and conversely for those specimens without the K-component in the larger IRM_{40mT}/χ_{ARM} values (Figure 11c). This indicates that the grains that may be carrying the K-component are not focused on either end of the magnetite particle size range. For the magnetite-dominated magnetization, the NRM intensity is related to magnetite abundance (as measured by either IRM_{40mT} or χ_{ARM}; Figure 11d), which is in turn strongly related to the siliciclastic content in the limestones (Hounslow, Cózar, et al., 2024). Perhaps importantly, the NRM intensity to IRM_{40mT} correlation improves (larger R^2) and steepens through the three categories in Figure 11d. These conditions suggest that the K-component is preferentially held by magnetic grains associated with the siliciclastic fraction.

One of the pitfalls of using laboratory remanences with sediments is that the laboratory magnetization may activate that proportion of the magnetic fraction which are not carrying the natural remanence. Here, the natural remanence is <0.4% of the IRM_{40mT} (Figure 11d) and <~0.2% for χ_{ARM} (χ_{ARM} = ~2x IRM_{40mT}). In addition, magnetic particle populations in siliciclastics tend to occur as both discrete fractions (not included in other detritals), and an included fraction, which is found in the much more abundant silicates (Franke et al., 2007; Hounslow & Maher, 1996; Hounslow & Morton, 2004), although the included fraction may not carry much natural remanence (Chang et al., 2016). These will respond differently to sulfidic diagenesis, with the discrete fraction being preferentially removed and the included fraction preferentially retained with greater sulfidic-related losses. The included fraction could therefore be a reservoir of Fe-oxides grains, which carry little or no natural remanence, but a potential larger reservoir of grains to acquire TVRM. Hence, a working hypothesis for the magnetization in these limestones, is that the ChRM component is largely carried by a discrete magnetic fraction (perhaps with some addition from Fe-oxide inclusions), and the K-component is disproportionately

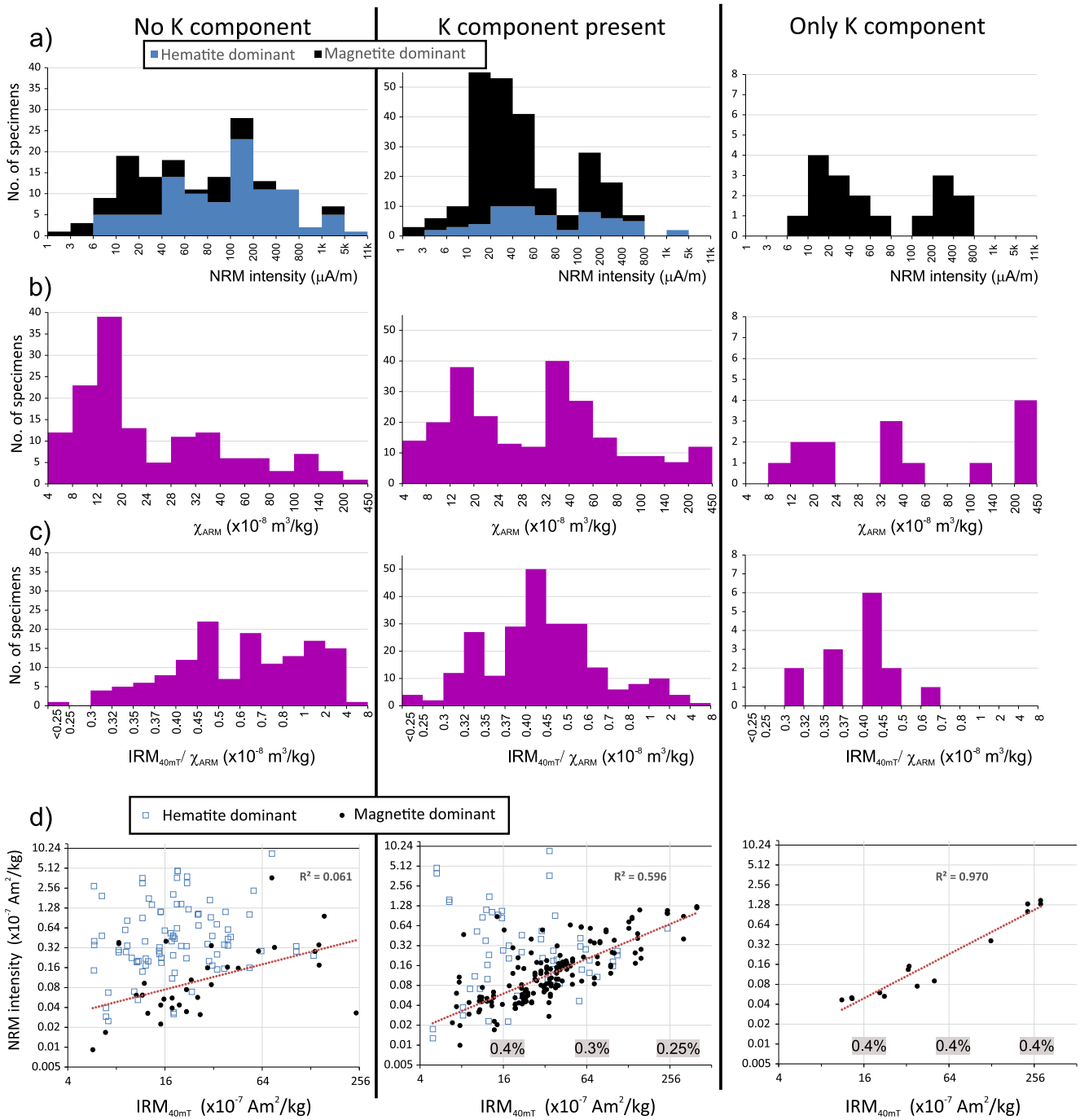

Figure 11. The K-component within the Trowbarrow specimens with respect to magnetic properties. In each column from left to right are displayed the specimens with left: no inferred K-component, mid: K-component was present with the ChRM, and right: specimens containing only the K-component and no ChRM. The first row, (a) shows specimens partitioned into NRM intensity and hematite and magnetite-dominated demagnetization behavior, second row, (b) specimens partition into χ_{ARM}, (c) specimens partitioned into the grain size proxy IRM_{40mT}/χ_{ARM} and (d) mass specific NRM intensity and IRM_{40mT}, with respect to hematite and magnetite-dominated demagnetization behavior. In (d) grayed values are the NRM/IRM_{40mT} as a percentage, using the regression fitted line (and Pearson R^2) to the magnetite-dominated data at IRM_{40mT} of 16, 64 and 256 × 10^{-7} A.m^2/kg. Rock magnetic data for (b) and (c) from Hounslow, Cózar, et al. (2024). Histogram intervals were chosen to give an approximate even spread through the whole respective datasets.

carried by the silicate-hosted fraction of hematite and magnetite as a TVRM. Diagenetic and siliciclastic source-controlled variations in the relative abundance of discrete and included Fe-oxides could therefore explain the variable preservation of the ChRM and K-component.

4.2. The Mineralogical Origin of the ChRM

The fold tests indicate that the ChRM component was acquired close to 100% untilting. This together with the VGP locations that are comparable to Mississippian volcanic VGP's (Figure 9), and the recovery of dual polarities suggests that the ChRM component is an Early Carboniferous magnetization.

A surprising feature in the Trowbarrow succession is the dominance of hematite as the carrier of the magnetization, which is more widespread than could be inferred from the localized reddening observed at many of the emergent surfaces. An estimate of the average weight% of hematite is 0.07% (min, max = 0.001, 1.1%; with S-ratio < -0.5) using a saturation remanence of 0.18 $A.m^2\ kg^{-1}$ (Peters and Dekkers, 2003). There are three possible sources for the hematite. First, as "terra-rossa type' residues associated with emergent surface development, as described by Wright et al. (1997). Such sourced grains would need to have percolated downwards through the carbonates via the pore networks during emergence to account for its presence meters below the emergent surfaces. However, a carbonate-hosted dissolution source for hematite as a residual phase has been discounted for modern carbonate systems, where the amount of limestone dissolution required is beyond realistic limits (Jones, 2021; Muhs and Budahn, 2009). Second, as eolian sourced material either from volcanic dust or as dust supplied from nearby desert margins (Jones, 2021). Sources of terrestrial dust could be nearby Visean uplands (Wakefield et al., 2016) or more far-field sources (McGlannan et al., 2022). Hounslow, Cózar, et al. (2024) have proposed this as the primary source of hematite in the Trowbarrow carbonates. Third, dispersal from coeval laterally present paleosols, since the carbonate ramp probably had some topography (e.g., Eberli, 2013), and also likely shallowed to the north against the Cumbrian high (Mitchell et al., 1978). In this scenario, the silty paleosol-tops would be prone to reworking during the immediately overlying flooding event, from which siliciclastics would be subsequently dispersed laterally into developing carbonate deposits.

Either of the latter two possibilities could produce detrital hematite carrying a primary Carboniferous magnetization. In contrast, the first option would generate a post-depositional (but early) magnetization timed to the overlying paleosol and emergence. Where the polarity changes across the emergent surface (i.e., at base of TQ2n, TQ2n.2n, TQ4n.1r, and TQ9n.2n), the underlying magnetozone is often rather thin. In this case, using the emergent-surface sourced scenario would suggest that any down-wards percolation of hematite was of limited vertical extent.

4.3. Magnetostratigraphic Comparisons

In Europe, the only detailed coeval magnetostratigraphy to that seen at Trowbarrow is from the lava succession at Kinghorn, near Kirkcaldy, Scotland (Wilson & Everitt, 1963; Torsvik et al., 1989; summarized in Hounslow, 2022). This lava succession is 390 m thick, with the First Abden Limestone immediately below the top-most lava, and the second Abden Limestone some 20 m above the uppermost lava. The First Abden Limestone is near the top of the early Brigantian, and the Second Abden Limestone is near the base of the Serpukhovian (Cózar & Somerville, 2020, 2021). The lowest part of the miospore *Bellispores nitidus—Reticulatisporites carnosus* (NC) Zone can be placed above the lava succession within the Second Abden Limestone (Brindley & Spinner, 1989; Owens et al., 2005). In northern England and Scotland, the base of this zone is typically in the mid Brigantian, with the underlying *Tripartites vetustus– Rotaspora fracta* (VF) Zone extending into the latest Asbian (McLean et al., 2018). A secure underlying marker at Kinghorn is the Birdiehouse Limestone (some 190 m below the base of the lavas; Figure 12), which is a well-defined marker in this region (Guirdham, 1998) in the lower part of the NM biozone (Brindley & Spinner, 1989; Rex & Scott, 1987), with the base of the NM biozone placed in the early Asbian (Owens et al., 2005). The strata between the Birdiehouse Limestone and the lower part of the Kinghorn Volcanics belong to the *Raistrickia nigra– Triquitrites marginatus* (NM) Biozone (Brindley & Spinner, 1989). The NM biozone is dated to most of the Asbian. Therefore, the top part of the lava succession should be early Brigantian with the Asbian-Brigantian boundary probably within the lava succession (Figure 12). The base of the lava succession is also within the Asbian, but at an uncertain position above or within the early Asbian.

The normal polarity dominance in the mid part of the Kinghorn Volcanic Fm concurs with that observed at Trowbarrow, although the likely sporadically erupted lavas are unlikely to express fine-scale polarity changes as at Trowbarrow. The reverse polarity in the upper part of the lava succession (inferred as MI5r in the GPTS; Figured 12) is not seen at Trowbarrow, which suggests that this reverse polarity interval is younger than the Brigantian limestones at Trowbarrow. It is probable that the reverse polarity intervals in the lowest part of the

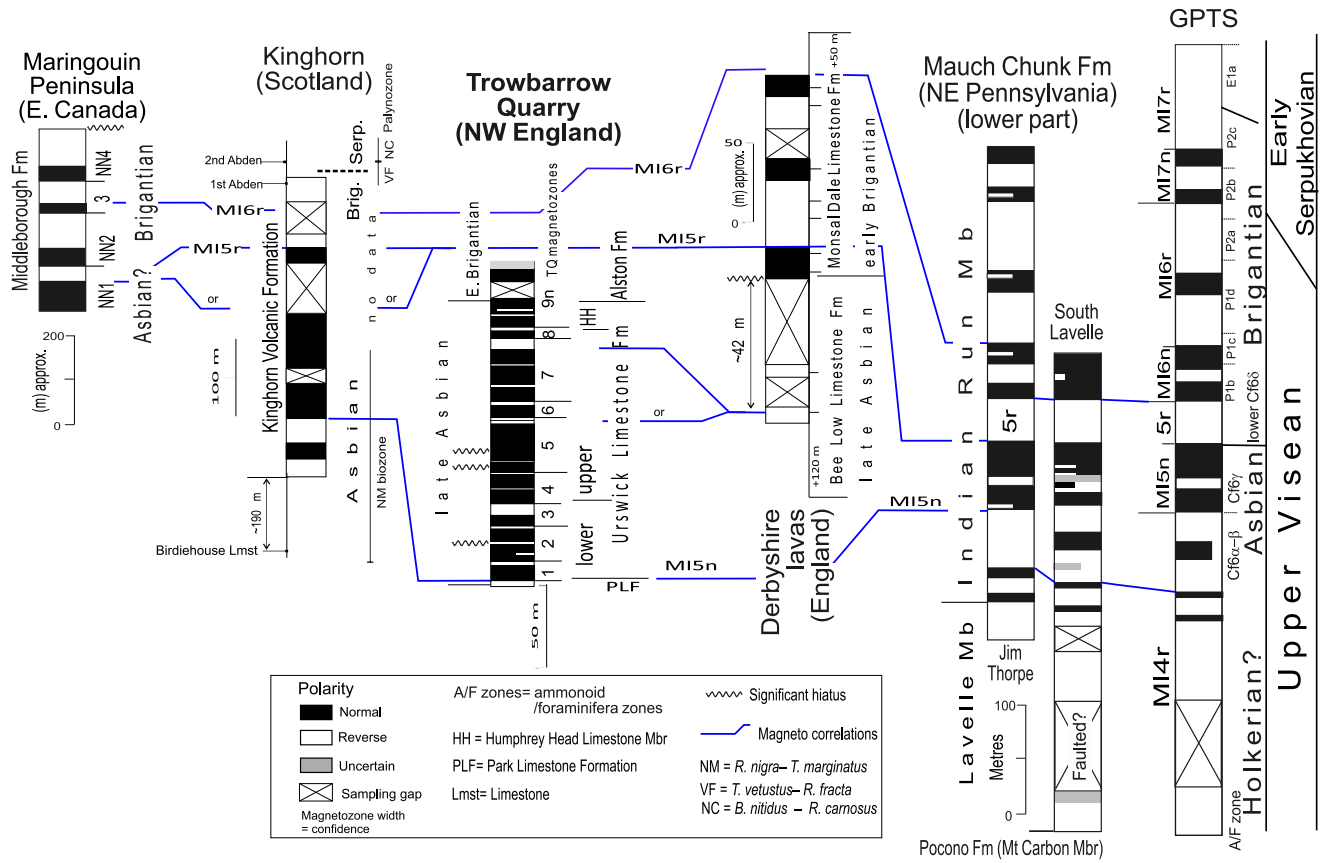

Figure 12. Comparison of the magnetostratigraphy at Trowbarrow Quarry with other sections of coeval age, and the geomagnetic polarity timescale (GPTS) of Hounslow (2022). Source data: Maringouin Peninsula (Opdyke et al., 2014), Kinghorn and Derbyshire (composites compiled in Hounslow, 2022), and Mauch Chunk Fm (Opdyke & DiVenere, 2004).

Kinghorn Volcanic Fm may relate to intervals in the early Asbian, coeval with the upper parts of the Park Limestone Fm, which have not yet been studied (Figures 1 and 12).

Upper Visean age lavas studied for paleomagnetism in Derbyshire are stratigraphically widely separated, and the normal polarity lavas in the base of the Monsal Dale Limestone Fm are probably coeval with the normal polarity interval seen at Trowbarrow in the basal Alston Fm (Figure 12). The lower and upper units of the Monsal Dale Limestone Fm contain corals indicating early Brigantian zones H and I of Mitchell (1989). Hence, the overlying reverse and normal polarity lavas in the Monsal Dale Limestone are early Brigantian in age (Waters et al., 2011b). The underlying Bee Low Limestone Fm contains goniatites, indicating the *Goniatites globostriatus* Subzone (B2b Subzone; Waters et al., 2011b) of the late Asbian. Likewise, foraminifera indicate the Cf6γ1b assemblage from the base of the formation, with probably assemblage Cf6γ2c missing and possibly the upperpart of Cf6γ2b also absent (Chisholm et al., 1983; Strank, 1985) The two levels of lava in the upper 20%–30% of the Bee Low Limestone show reverse polarity (Figure 12), and may relate to the reverse polarity intervals TQ6r and TQ7r. However, without a study of the remainder of the Bee Low Limestone the magnetostratigraphic correlation remains uncertain for these two lower lavas.

In eastern Canada, the magnetostratigraphy from the Middleborough Fm (Figure 12) is inferred to be Brigantian in age based on the late Asbian age for the underlying Limekiln Brook Fm (Giles, 2008; Jutras et al., 2016; Utting et al., 2010). However, since the Limekiln Brook Fm is laterally transitional into the lower part of the Middleborough Fm (Jutras et al., 2016), it is possible that the oldest part of the magnetostratigraphy of Opdyke et al. (2014), consisting of magnetozones NN1–NN2, may extend into the late Asbian rather than being entirely Brigantian (Figure 12). This latter option is compatible with the magnetostratigraphy indicating that the NN1r-NN2n magnetozone interval could be coeval with an interval low in the early Brigantian with NN1n probably equivalent to the basal Brigantian as seen at Trowbarrow (Figure 12).

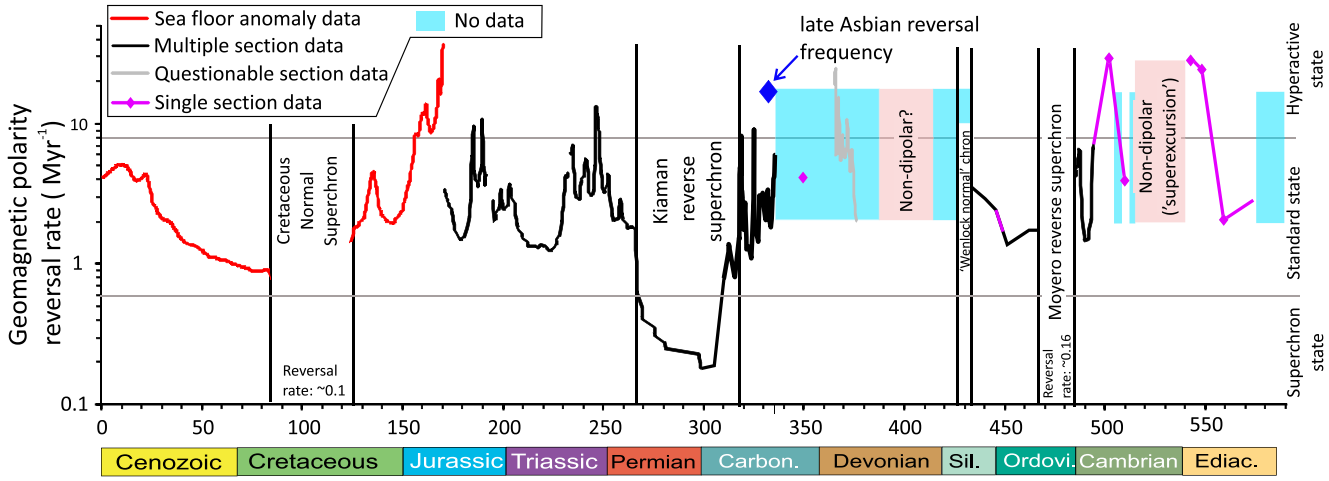

Figure 13. Geomagnetic polarity reversal rates through the Phanerozoic and the Ediacaran (adapted from Hounslow et al., 2018; Ogg & Hounslow, 2022). Reversal frequency for the late Asbian in Trowbarrow Quarry is also shown. The lower reversal rates for the coeval part of the Carboniferous derive from the Mauch Chunk Fm and the timescale in Hounslow (2022). Ediac. = Ediacaran, Ordovi. = Ordovician, Sil. = Silurian, Carbon. = Carboniferous.

The magnetostratigraphy from the Mauch Chunk Fm in NE Pennsylvania (DiVenere & Opdyke, 1991; Opdyke & DiVenere, 2004) extends in age from near the top of the Chesterian (~323 Ma), to either: a) near the base of the Chesterian (~335 Ma) or b) extends into the Meramecian (base ~ 343 Ma). These are the short (e.g., Brezinski & Kollar, 2021) and long (e.g., Ettensohn et al., 2022) duration options for the Mauch Chunk Fm of NE Pennsylvanian discussed by Hounslow (2022). Based on the arguments presented by Opdyke et al. (2014) and Hounslow (2022), the most likely position for the top of the magnetostratigraphy from the Mauch Chunk Fm (not shown in Figure 12) is near the base of the early Bashkirian. Based on similarity in the reversal pattern between the palynologically dated Brigantian from eastern Canada and that from the upper part of the Indian Run Mbr of the Mauch Chunk, Hounslow (2022) suggested that the most likely option was that the mid parts of the Kinghorn Volcanic Fm were coeval with the predominantly normal polarity interval referred to as magnetochron MI5n, derived from the Mauch Chunk dataset (Figure 12). The data from Trowbarrow now more firmly assign this thicker normal polarity interval to the late Asbian. The equivalent interval to magnetochron MI5n was sampled in the Mauch Chunk Fm at two sections in the lower part of the Indian Run Mb (Figure 12). It was defined by results from 19 levels in one section and 18 levels in the other. In comparison, the late Asbian succession in Trowbarrow displays a much more detailed polarity pattern due to our higher sampling density. This additional complexity of MI5n is perhaps partly reflected (but there unresolved) in the multiple single-sample submagnetozones detected in MI5n by Opdyke & DiVenere (2004).

The astrochronology from Trowbarrow (Hounslow, Cózar, et al., 2024) indicates that the late Asbian has a duration of 1.976 ± 0.086 Myr (1σ), including 3 significant hiatus levels (marked on Figure 12). This duration is within the uncertainty from radioisotopic dates spanning this interval. The duration estimate and its uncertainty include three magnetic proxies from two separate equally likely sedimentation rate models (i.e., six estimates). Uncertainty in the period of the eccentricity targets used in the astrochronology adds some 1.5%–1.9% additional uncertainty (~0.037 Myr; Hounslow, Cózar, et al., 2024), which gives a combined 1σ uncertainty of 0.094 Myr. Quantifying duration uncertainty beyond this is challenging but could come from using multiple astrochronologic techniques (e.g., Da Silva et al., 2020) or multiple coeval overlapping sections (Sinnesael et al., 2019).

This duration translates to a polarity reversal frequency of 15.7 ± 0.75 Myr^{-1} (TQ1n-TQ9n.2n; excluding the tentative submagnetozones). Evidently, the lower reversal frequency, largely estimated with the datasets from the Mauch Chunk Fm through this interval, is an underestimate (black curve in Figure 13). However, the data from the Mauch Chunk Fm does not indicate a high reversal frequency in either under or overlying strata. Hence, it is possible that the interval with hyperactive-reversals is a stratigraphically restricted interval, like that which occurs in the Triassic and Lower Jurassic at around 246–248 Ma and 190–192 Ma, respectively (Figure 13). This brevity is rather different from the Cambrian and Ediacaran, which seem to have more sustained intervals of high reversal

frequency and corresponding weak paleointensity, which particularly characterize the Middle Jurassic (Kulakov et al., 2019) and the Late Ediacaran (Levashova et al., 2021; Thallner et al., 2022; Figure 13).

However, a middle Visean high reversal frequency seems compatible with current datasets from the Late Devonian (gray curve in Figure 13; Green et al., 2021; curve from Hounslow, 2022). It is further consistent with the very low paleointensity estimates recovered from the coeval Kinghorn Volcanics that define the youngest point of the "mid-Paleozoic Dipole Low" (Hawkins et al., 2021). The fact that the mid-Paleozoic is temporally equidistant to the Middle Jurassic and the Late Ediacaran is suggestive of a ∼200 Myr quasi-cyclicity in paleomagnetic field behavior (Biggin et al., 2012). Such long-term variations remain to be convincingly explained but may be linked to changes in subduction flux (Hounslow et al., 2018), true polar wander (van der Boon et al., 2022) and/or mantle plume events Biggin et al. (2012). As highlighted by Van der Boon et al. (2022), the Earth's magnetic field behavior during the Early Carboniferous and Devonian is key to consolidating hypotheses about the causes and implications of the Phanerozoic behavior of the geodynamo.

5. Conclusions

A magnetic polarity stratigraphy has been evaluated through the late Asbian type section in Trowbarrow Quarry, covering the top-most early Asbian through to the earliest Brigantian (ca. 334.5–332.5 Ma). This is tied to a detailed foraminiferal biostratigraphy and an astrochronology. The magnetostratigraphy yields nine major magnetozone couplets, seven minor submagnetozones and two tentative submagnetozones through the 195 m of section.

The magnetization is carried by hematite and in some samples a likely detrital magnetite phase. The hematite is probably of aeolian origin but also perhaps with some pedogenic-derived hematite associated with some of the 13 major emergent surfaces. A regional fold test using data from fourteen, other largely Visean localities studied in NW England, indicates that ChRM magnetization was of pre-tilting age so prior to the Late Pennsylvanian to Early Permian.

The Mississippian age magnetization is partly overprinted with Kiaman Superchron-age (ca. 320–270 Ma) and Brunhes-age (0.77–0 Ma) magnetization, which are inferred to be thermoviscous in origin. Regional fold tests using the Cumbrian and north Lancashire sections indicate that the Kiaman age partial remagnetization is younger than the principal Variscan age folding, so probably of the latest Pennsylvanian to early Permian age.

The polarity stratigraphy defines many short-duration submagnetochrons in the Mississippian magnetochron MI5n. A reversal rate of 15.7 ± 0.75 Myr^{-1} is inferred for the late Asbian, indicating that at ca. 335–333 Ma the geodynamo was in a state of hyperactive reversal.

Data Availability Statement

The data used for this study, both the raw measurements and the interpretation matrix, are available at the Figshare data repository (Hounslow, Biggin, et al., 2024). The software used is also available on the Figshare data repository (Hounslow, 2019, 2023a, 2023b).

Acknowledgments
MWH, TK, AB and CJS were in part funded by NERC (Grant NE/P00170X/1) and the Leverhulme Trust (RLA-2016-080). Vassil Karloukovski, David Mindham and Ondřej Sysel helped collect samples. Emma Gray, Estibaliz Leibar Porcel, David Mindham and Vassil Karloukovski helped prepare and measure much of the Trowbarrow dataset. Samples for $\delta^{13}C$, $\delta^{18}O$ were measured by Dave Hughes at Lancaster. Natural England, the Arnside Silverdale AONB, Lancaster City Council, Cumbria Wildlife Trust, Holker Hall Estate and the Landowners of Crosthwaite and Lyth allowed access, permission and permits to collect samples from these sections. Two anonymous reviewers assisted improvements in the text.

References

Adams, A. E., Horbury, A. D., & Abdel Aziz, A. A. (1990). Controls on Dinantian sedimentation in south Cumbria and surrounding areas of northwest England. *Proceedings of the Geologists' Association*, *101*(1), 19–30. https://doi.org/10.1016/S0016-7878(08)80203-9

Addison, F. T., Turner, P., & Tarling, D. H. (1985). Magnetic studies of the Pendleside Limestone: Evidence for re-magnetisation and late diagenetic dolomitisation during a post Asbian normal event. *Journal of the Geological Society*, *142*(6), 983–994. https://doi.org/10.1144/gsjgs.142.6.0983

Aretz, M., Herbig, H. G., & Wang, X. D. (2020). The Carboniferous Period. In F. M. Gradstein, J. G. Ogg, M. D. Schmitz, & G. M. Ogg (Eds.), *Geologic time scale 2020* (pp. 811–873). Elsevier. https://doi.org/10.1016/B978-0-12-824360-2.00023-1

Barnett, A. J., Burgess, P. M., & Wright, V. P. (2002). Icehouse world sea-level behaviour and resulting stratal patterns in late Visean (Mississippian) carbonate platforms: Integration of numerical forward modelling and outcrop studies. *Basin Research*, *14*(3), 417–438. https://doi.org/10.1046/j.1365-2117.2002.00186.x

Biggin, A. J., Steinberger, B., Aubert, J., Suttie, N., Holme, R., Torsvik, T. H., et al. (2012). Possible links between long-term geomagnetic variations and whole-mantle convection processes. *Nature Geoscience*, *5*(8), 526–533. https://doi.org/10.1038/ngeo1521

Brandon, A., Aitkenhead, N., Croft, R. G. C., Ellison, R. A. E., Evans, D. J. & Riley, N. J. (1998). *Geology of the country around Lancaster: Memoir for 1: 50 000 geological sheet 59 (England and Wales) (No. 59). British geological survey*. HMSO.

Brezinski, D. K., & Kollar, A. D. (2021). Lithofacies and fauna of the Loyalhanna Limestone (Chesterian, Upper Mississippian) and their implications for its origin in the Appalachian Basin. *Annales Carnegie Museum*, *87*(2), 139–156. https://doi.org/10.2992/007.087.0203

Brindley, S., & Spinner, E. (1989). Palynological assemblages from Lower Carboniferous deposits, Burntisland district, Fife, Scotland. *Proceedings of the Yorkshire Geological Society*, *47*(3), 215–231. https://doi.org/10.1144/pygs.47.3.215

Burnett, R. D. (1987). Regional maturation patterns for late Visean (Carboniferous, Dinantian) rocks of northern England based on mapping of conodont colour. *Irish Journal of Earth Sciences*, *8*, 165–185.

Chang, L., Roberts, A. P., Heslop, D., Hayashida, A., Li, J., Zhao, X., et al. (2016). Widespread occurrence of silicate-hosted magnetic mineral inclusions in marine sediments and their contribution to paleomagnetic recording. *Journal of Geophysical Research: Solid Earth*, *121*(12), 8415–8431. https://doi.org/10.1002/2016JB013109

Channell, J. E. T., McCabe, C., & Woodcock, N. H. (1992). Early Devonian (pre-Acadian) magnetization directions in the Lower Old Red Sandstone of south Wales (UK). *Geophysical Journal International*, *108*(3), 883–894. https://doi.org/10.1111/j.1365-246X.1992.tb03477.x

Chisholm, J. I., Mitchell, M., Strank, A. R. E., Cox, F. C., & Harrison, D. J. (1983). *A revision of the stratigraphy of the Asbian and Brigantian limestones of the area west of Matlock, Derbyshire. Report of the Institute of Geological Science* (Vol. 83/10, pp. 17–24). HMSO.

Cózar, P., Coronado, I., Somerville, I. D., & Hounslow, M. W. (2023b). High-resolution definition and correlation of the Asbian–Brigantian boundary in northern England and the Scottish borders, using foraminiferal diversity and richness. *Proceedings of the Yorkshire Geological Society*, *64*(3–4). https://doi.org/10.1144/pygs2023-003

Cózar, P., & Somerville, I. D. (2004). New algal and foraminiferal assemblages and evidence for recognition of the Asbian–Brigantian boundary in northern England. *Proceedings of the Yorkshire Geological Society*, *55*(1), 43–65. https://doi.org/10.1144/pygs.55.1.43

Cózar, P., & Somerville, I. D. (2005). Significance of calcareous algae for the recognition of the Asbian and Brigantian Stages (Mississippian) in Ireland and Great Britain. *Revista Espanola de Micropaleontologia*, *37*, 71–94.

Cózar, P., & Somerville, I. D. (2020). Foraminiferal biostratigraphy of Brigantian-Arnsbergian limestones from eastern Scotland and Northumberland (northeast England). *Earth and Environmental Sciences, Transactions of the Royal Society Edinburgh*, *111*(3), 193–207. https://doi.org/10.1017/S1755691020000092

Cózar, P., & Somerville, I. D. (2021). The Serpukhovian in Britain: Use of foraminiferal assemblages for dating and correlating. *Journal of the Geological Society*, *178*(3). https://doi.org/10.1144/jgs2020-17

Cózar, P., Somerville, I. D., & Hounslow, M. W. (2022a). Foraminifers in the Holkerian Stratotype, regional substage in Britain: Key taxa for the Viséan subdivision. *Newsletters on Stratigraphy*, *55*(2), 159–172. https://doi.org/10.1127/nos/2021/0674

Cózar, P., Somerville, I. D., & Hounslow, M. W. (2023a). A potential global chronostratigraphic boundary for the base of the middle Viséan. *Newsletters on Stratigraphy*, *56*(3), 357–376. http://doi.org/10.1127/nos/2023/0746

Cózar, P., Somerville, I. D., Hounslow, M. W., & Coronado, I. (2022c). Far-field correlation of palaeokarstic surfaces in Mississippian successions using high-frequency foraminiferal diversity trends. *Palaeogeography, Palaeoclimatology, Palaeoecology*, *601*, 111088. http://doi.org/10.1016/j.palaeo.2022.111088

Cózar, P., Somerville, I. D., Hounslow, M. W., & Kamenikova, T. (2022b). A late Asbian (Mississippian) stratotype for England: Trowbarrow Quarry, Cumbria, UK. *Papers in Palaeontology*, *8*(3). https://doi.org/10.1002/spp2.1451

Crowley, S. F., Piper, J. D., Bamarouf, T., & Roberts, A. P. (2014). Palaeomagnetic evidence for the age of the Cumbrian and Manx hematite ore deposits: Implications for the origin of hematite mineralization at the margins of the east Irish Sea Basin, UK. *Journal of the Geological Society*, *171*(1), 49–64. https://doi.org/10.1144/jgs2013-004

Da Silva, A. C., Sinnesael, M., Claeys, P., Davies, J. H., de Winter, N. J., Percival, L. M. E., et al. (2020). Anchoring the Late Devonian mass extinction in absolute time by integrating climatic controls and radio-isotopic dating. *Scientific Reports*, *10*(1), 12940. https://doi.org/10.1038/s41598-020-69097-6

Davis, W., & Buffett, B. (2022). Inferring core processes using stochastic models of the geodynamo. *Geophysical Journal International*, *228*(3), 1478–1493. https://doi.org/10.1093/gji/ggab412

Deenen, M. H., Langereis, C. G., van Hinsbergen, D. J., & Biggin, A. J. (2014). Erratum: Geomagnetic secular variation and the statistics of palaeomagnetic directions. *Geophysical Journal International*, *197*(1), 643. https://doi.org/10.1093/gji/ggu021

DiVenere, V. J., & Opdyke, N. D. (1991). Magnetic polarity stratigraphy in the uppermost Mississippian Mauch Chunk formation, Pottsville, Pennsylvania. *Geology*, *19*(2), 127–130. https://doi.org/10.1130/0091-7613(1991)019<0127:MPSITU>2.3.CO;2

Dunlop, D. J. (1983). Determination of domain structure in igneous rocks by alternating field and other methods. *Earth and Planetary Science Letters*, *63*(3), 353–367. https://doi.org/10.1016/0012-821X(83)90109-7

Dunlop, D. J., Özdemir, Ö., & Schmidt, P. W. (1997). Paleomagnetism and paleothermometry of the Sydney Basin 2. Origin of anomalously high unblocking temperatures. *Journal of Geophysical Research*, *102*(B12), 27285–27295. https://doi.org/10.1029/97JB02478

Eberli, G. P. (2013). The uncertainties involved in extracting amplitude and frequency of orbitally driven sea-level fluctuations from shallow-water carbonate cycles. *Sedimentology*, *60*(1), 64–84. https://doi.org/10.1111/sed.12011

Elmore, R. D., Muxworthy, A. R., & Aldana, M. (2012). Remagnetization and chemical alteration of sedimentary rocks. In R. D. Elmore, A. R. Muxworthy, M. M. Aldana, & M. Mena (Eds.), *Remagnetization and chemical alteration of sedimentary rocks*, *Geological Society, London, Special Publications* (Vol. 371, pp. 1–21).

Enkin, R. J. (2003). The direction–correction tilt test: An all-purpose tilt/fold test for paleomagnetic studies. *Earth and Planetary Science Letters*, *212*(1–2), 151–166. https://doi.org/10.1016/s0012-821x(03)00238-3

Enkin, R. J., & Watson, G. S. (1996). Statistical analysis of palaeomagnetic inclination data. *Geophysical Journal International*, *126*(2), 495–504. https://doi.org/10.1111/j.1365-246X.1996.tb05305.x

Ettensohn, F. R., Gilliam, W., Li, J., & Zeng, M. (2022). Timing and evolution of the Mississippian sedimentary system on southeastern Laurussia: Evidence from the Appalachian area, USA. *Palaeogeography, Palaeoclimatology, Palaeoecology*, *591*, 110874. https://doi.org/10.1016/j.palaeo.2022.110874

Frank, U., & Nowaczyk, N. R. (2008). Mineral magnetic properties of artificial samples systematically mixed from haematite and magnetite. *Geophysical Journal International*, *175*(2), 449–461. https://doi.org/10.1111/j.1365-246X.2008.03821.x

Franke, C., von Dobeneck, T., Drury, M. R., Meeldijk, J. D., & Dekkers, M. J. (2007). Magnetic petrology of equatorial Atlantic sediments: Electron microscopy results and their implications for environmental magnetic interpretation. *Paleoceanography*, *22*(4). https://doi.org/10.1029/2007PA001442

Fraser, A. J., & Gawthorpe, R. L. (2003). *An atlas of Carboniferous basin evolution in northern England* (Vol. 28). Geological Society London.

Gallet, Y., Pavlov, V., & Korovnikov, I. (2019). Extreme geomagnetic reversal frequency during the Middle Cambrian as revealed by the magnetostratigraphy of the Khorbusuonka section (northeastern Siberia). *Earth and Planetary Science Letters*, *528*, 115823. https://doi.org/10.1016/j.epsl.2019.115823

Giles, P. S. (2008). Windsor group (Late Mississippian) stratigraphy, Magdalen Islands, Quebec: A rare eastern Canadian record of late Visean basaltic volcanism. *Atlantic Geology*, *44*, 167–185. https://doi.org/10.4138/5932

Green, T., Slotznick, S. P., Jaqueto, P., Raub, T. D., Tohver, E., Playton, T. E., et al. (2021). High-Resolution Late Devonian Magnetostratigraphy from the Canning Basin, Western Australia: A re-evaluation. *Frontiers in Earth Science*, *9*. https://doi.org/10.3389/feart.2021.757749

Guirdham, C. (1998). Regional stratigraphy, lithofacies, diagenesis and dolomitisation of microbial carbonates in the Lower Carbonifereous, West Lothian Oil-Shale Formation (Doctoral dissertation). *University of East Anglia*.

Hawkins, L., Grappone, J. M., Sprain, C. J., Saengduean, P., Sage, E. J., Thomas-Cunningham, S., et al. (2021). Intensity of the Earth's magnetic field: Evidence for a Mid-Paleozoic dipole low. *Proceedings of the National Academy of Sciences*, *118*(34), e2017342118. https://doi.org/10.1073/pnas.2017342118

Heslop, D., & Roberts, A. P. (2016). Estimation and propagation of uncertainties associated with paleomagnetic directions. *Journal of Geophysical Research: Solid Earth*, *121*(4), 2274–2289. https://doi.org/10.1002/2015JB012544

Horbury, A. D. (1987). *The sedimentology of the Urswick Limestone in south Cumbria and north Lancashire, (Doctoral dissertation)*. University of Manchester.

Horbury, A. D. (1989). The relative roles of tectonism and eustacy in the deposition of the Urswick Limestone in south Cumbria and north Lancashire. In R. S. Arthurton, P. Gutteridge, & S. C. Nolan (Eds.), *The role of tectonics in Devonian and Carboniferous sedimentation in the British Isles* (Vol. 6, pp. 153–169). Yorkshire Geological Society Occasional Publication.

Horbury, A. D., & Adams, A. E. (1996). Microfacies association in Asbian carbonates: An example from the Urswick Limestone Formation of the southern Lake District, northern England. In P. Strogen, I. D. Somerville, & G. L. Jones (Eds.), *Recent advances in lower carboniferous geology*, *Geological Society, London, Special Publications* (Vol. 107, pp. 222–237).

Hounslow, M. W. (2019). GM4Edit (v.5.6) – a windows program to manage, plot, export and manipulate palaeomagnetic magnetometer datasets [Software]. https://doi.org/10.13140/RG.2.2.31877.91361/1

Hounslow, M. W. (2022). A geomagnetic polarity timescale for the Carboniferous. In S. G. Lucas, J. W. Schneider, X. Wang, & S. Nikolaeva (Eds.), *The Carboniferous Timescale* (Vol. 512, pp. 141–195). Geological Society, London, Special Publications. https://doi.org/10.1144/SP512-2020-102

Hounslow, M. W. (2023a). A DosBox version of LINEFIND of Kent, Briden and Mardia (1983) [Software]. *figshare*. https://doi.org/10.6084/m9.figshare.24826617

Hounslow, M. W. (2023b). Palaeomag-Tools, version 5.1a- a tool for analysis of 2-D and 3-D directional data [Software]. *figshare*. https://doi.org/10.6084/m9.figshare.24167190.v1

Hounslow, M. W., Biggin, A. J., Cózar, P., Somerville, I. D., Kamenikova, T., & Sprain, C. J. (2024). Palaeomagnetic dataset for Trowbarrow Quarry section, and additional sites in South Cumbria and north Lancashire [Dataset]. *figshare*. https://doi.org/10.6084/m9.figshare.24162549

Hounslow, M. W., Cózar, P., Somerville, I. D., & Biggin, A. J. (2024). Rock magnetic-based cyclic expression in late Visean ramp carbonates and an astrochronology for the late Asbian from Northwest England. *Paleoceanography and Paleoclimatology*, *39*(3), e2023PA004772. https://doi.org/10.1029/2023PA004772

Hounslow, M. W., Domeier, M., & Biggin, A. J. (2018). Subduction flux modulates the geomagnetic polarity reversal rate. *Tectonophysics*, *742*, 34–49. https://doi.org/10.1016/j.tecto.2018.05.018

Hounslow, M. W., Horng, C. S., & Karloukovski, V. (2023). Rotational remanent magnetization as a magnetic mineral diagnostic tool at low rotation rates. *Geophysical Journal International*, *232*(1), 300–321. https://doi.org/10.1093/gji/ggac330

Hounslow, M. W., & Maher, B. A. (1996). Quantitative extraction and analysis of carriers of magnetization in sediments. *Geophysical Journal International*, *124*(1), 57–74. https://doi.org/10.1111/j.1365-246X.1996.tb06352.x

Hounslow, M. W., & Morton, A. C. (2004). Evaluation of sediment provenance using magnetic mineral inclusions in clastic silicates: Comparison with heavy mineral analysis. *Sedimentary Geology*, *171*(1–4), 13–36. https://doi.org/10.1016/j.sedgeo.2004.05.008

Hounslow, M. W., Posen, P. E., & Warrington, G. (2004). Magnetostratigraphy and biostratigraphy of the Upper Triassic and lowermost Jurassic succession, St. Audrie's Bay, UK. *Palaeogeography, Palaeoclimatology, Palaeoecology*, *213*(3–4), 331–358. https://doi.org/10.1016/j.palaeo.2004.07.018

Hounslow, M. W., Xuan, C., & Nilsson, A. (2022). Chapter 5: Using the geomagnetic field for correlation and dating. In A. L. Coe (Ed.), *Deciphering Earth's history: The practice of stratigraphy* (pp. 81–99). Geological Society of London.

Johnson, E. W., Soper, N. J., & Burgess, I. C. (2001). *Geology of the country around Ulverston. Memoir of the British Geological Survey, Sheet 48 (England and Wales)*. HMSO.

Jones, B. (2021). Formation, dispersion and accumulation of terra rossa on the Cayman Islands. *Sedimentology*, *68*(5), 1964–2008. https://doi.org/10.1111/sed.12841

Jutras, P., McLeod, J., MacRae, R. A., & Utting, J. (2016). Complex interplay of faulting, glacioeustatic variations and halokinesis during deposition of upper Visean units over thick salt in the western Cumberland Basin of Atlantic Canada. *Basin Research*, *28*(4), 483–506. https://doi.org/10.1111/bre.12119

Kent, D. V. (1985). Thermoviscous remagnetization in some Appalachian limestones. *Geophysical Research Letters*, *12*, 805–808. https://doi.org/10.1029/GL012i012p00805

Kirby, G. A., Baily, H. E., Chadwick, R. A., Evans, D. J., Holliday, D. W., Holloway, S., et al. (2000). *The structure and evolution of the Craven Basin and adjacent areas*. Subsurface Memoir of the British Geological Survey.

Kulakov, E. V., Sprain, C. J., Doubrovine, P. V., Smirnov, A. V., Paterson, G. A., Hawkins, L., et al. (2019). Analysis of an updated paleointensity database (QPI-PINT) for 65-200 Ma: Implications for the long-term history of dipole moment through the Mesozoic. *Journal of Geophysical Research*, *124*(10), 9999–10022. https://doi.org/10.1029/2018JB017287

Levashova, N. M., Golovanova, I. V., Rudko, D. V., Danukalov, K. N., Rudko, S. V., Yu, S. R., & Meert, J. G. (2021). Late Ediacaran magnetic field hyperactivity: Quantifying the reversal frequency in the Zigan Formation, Southern Urals, Russia. *Gondwana Research*, *94*, 133–142. https://doi.org/10.1016/j.gr.2021.02.018

McCabe, C., & Channell, J. E. T. (1994). Late Paleozoic remagnetization in limestones of the Craven Basin (northern England) and the rock magnetic fingerprint of remagnetized sedimentary carbonates. *Journal of Geophysical Research*, *99*(B3), 4603–4612. https://doi.org/10.1029/93JB02802

McFadden, P. L. (1998). The fold test as an analytical tool. *Geophysical Journal International*, *135*(2), 329–338. https://doi.org/10.1046/j.1365-246X.1998.00640.x

McFadden, P. L., & McElhinny, M. W. (1988). The combined analysis of remagnetization circles and direct observations in palaeomagnetism. *Earth and Planetary Science Letters*, *87*(1–2), 161–172. https://doi.org/10.1016/0012-821X(88)90072-6

McFadden, P. L., & McElhinny, M. W. (1990). Classification of the reversal test in palaeomagnetism. *Geophysical Journal International*, *103*(3), 725–729. https://doi.org/10.1111/j.1365-246X.1990.tb05683.x

McFadden, P. L., & Schmidt, P. W. (1986). The accumulation of palaeomagnetic results from multicomponent analyses. *Geophysical Journal International*, *86*(3), 965–979. https://doi.org/10.1111/j.1365-246X.1986.tb00670.x

McGlannan, A. J., Bonar, A., Pfeifer, L., Steinig, S., Valdes, P., Adams, S., et al. (2022). An eolian dust origin for clastic fines of Devono-Mississippian mudrocks of the greater North American midcontinent. *Journal of Sedimentary Research*, *92*(12), 1186–1206. https://doi.org/10.2110/jsr.2022.013

McLean, D., Owens, B., Bodman, D. J., & McLean, F. D. (2018). Miospores from the Brigantian stratotype section at Janny Wood, Cumbria. *Proceedings of the Yorkshire Geological Society*, *62*(2), 89–100. https://doi.org/10.1144/pygs2017-004

Metcalfe, I., & Riley, N. J. (2010). Conodont colour alteration pattern in the Carboniferous of the Craven Basin and adjacent areas, northern England. *Proceedings of the Yorkshire Geological Society*, *58*, 1–8. https://doi.org/10.1144/pygs.58.1.265

Miller, K. G., & Wright, J. D. (2017). Success and failure in Cenozoic global correlations using golden spikes: A geochemical and magneto-stratigraphic perspective. *Episodes*, *40*(1), 8–21. https://doi.org/10.18814/epiiugs/2017/v40i1/017003

Mitchell, M. (1989). The biostratigraphy of Visean (Dinantian) rugose coral faunas from Britain. *Proceedings of the Yorkshire Geological Society*, *47*(3), 233–247. https://doi.org/10.1144/pygs.47.3.233

Mitchell, M., Taylor, B. J., & Ramsbottom, W. H. C. (1978). Carboniferous. In F. Moseley (Ed.), *The geology of the Lake District* (Vol. 3, pp. 168–188). Yorkshire Geological Society Occasional Publication.

Montgomery, P., Hailwood, E. A., Gale, A. S., & Burnett, J. A. (1998). The magnetostratigraphy of Coniacian-Late Campanian Chalk sequences in southern England. *Earth and Planetary Science Letters*, *156*(3–4), 209–224. https://doi.org/10.1016/S0012-821X(98)00008-9

Morris, P. (1971). Two component magnetisation in Irish Carboniferous limestone. *Earth and Planetary Science Letters*, *12*(3), 350–354. https://doi.org/10.1016/0012-821X(71)90221-4

Morris, P. (1972). Palaeomagnetic evidence for the rotation of North Co. Dublin. *Proceedings of the Royal Irish Academy B*, *72*, 221–227.

Moskowitz, B. M., Frankel, R. B., & Bazylinski, D. A. (1993). Rock magnetic criteria for the detection of biogenic magnetite. *Earth and Planetary Science Letters*, *120*(3–4), 283–300. https://doi.org/10.1016/0012-821X(93)90245-5

Muhs, D. R., & Budahn, J. R. (2009). Geochemical evidence for African dust and volcanic ash inputs to terra rossa soils on carbonate reef terraces, northern Jamaica, West Indies. *Quaternary International*, *196*(1–2), 13–35. https://doi.org/10.1016/j.quaint.2007.10.026

Nie, J., Ren, X., Saylor, J. E., Su, Q., Horton, B. K., Bush, M. A., et al. (2020). Magnetic polarity stratigraphy, provenance, and paleoclimate analysis of Cenozoic strata in the Qaidam Basin, NE Tibetan Plateau. *Geological Society of America Bulletin*, *132*(1–2), 310–320. https://doi.org/10.1130/B35175.1

Ogg, J. G., & Hounslow, M. W. (2022). Phanerozoic geomagnetic polarity time scale: Status, potential mega-trends, and challenges. In *AGU 2022 abstract*. Retrieved from agu.confex.com/agu/fm22/meetingapp.cgi/Paper/1093030

Oldfield, F. (1999). Environmental magnetism: The range of applications. In J. Walden, F. Oldfield, & J. Smith (Eds.), *Environmental magnetism, a practical guide, Quaternary Research Association, technical guide* (Vol. 6, pp. 212–223). Quaternary Research Association.

Opdyke, N. D., & DiVenere, V. J. (2004). The magnetic polarity stratigraphy of the Mauch Chunk Formation, Pennsylvania. *Proceedings of the National Academy of Sciences*, *101*(37), 13423–13427. https://doi.org/10.1073/pnas.0403786101

Opdyke, N. D., Giles, P. S., & Utting, J. (2014). Magnetic polarity stratigraphy and palynostratigraphy of the Mississippian-Pennsylvanian boundary interval in eastern North America and the age of the beginning of the Kiaman. *Geological Society of America Bulleting*, *126*(7–8), 1068–1083. https://doi.org/10.1130/B30953.1

Owens, B., McLean, D., Simpson, K. R. M., Shell, P. M. J., & Robinson, R. (2005). Re-appraisal of the Mississippian palynostratigraphy of the east Fife coast, Scotland, United Kingdom. *Palynology*, *29*(1), 23–47. https://doi.org/10.1080/01916122.2005.9989603

Palmer, J. A. (1987). *Carboniferous magnetostratigraphy, (Doctoral dissertation)*. University of Newcastle.

Pavlov, V. E., Pasenko, A. M., Shatsillo, A. V., Powerman, V. I., Shcherbakova, V. V., & Malyshev, S. V. (2018). Systematics of Early Cambrian paleomagnetic directions from the northern and eastern regions of the Siberian Platform and the problem of an anomalous geomagnetic field in the time vicinity of the Proterozoic–Phanerozoic boundary. *Izvestiya - Physics of the Solid Earth*, *54*(5), 782–805. https://doi.org/10.1134/S1069351318050117

Peters, C. (1995). *Unravelling magnetic mixtures in sediments, soils and rocks, (Doctoral dissertation)*. University of Edinburgh.

Peters, C., & Dekkers, M. J. (2003). Selected room temperature magnetic parameters as a function of mineralogy, concentration and grain size. *Physics and Chemistry of the Earth, Parts A/B/C 28*, *28*(16–19), 659–667. https://doi.org/10.1016/S1474-7065(03)00120-7

Peters, C., & Thompson, R. (1998). Magnetic identification of selected natural iron oxides and sulphides. *Journal of Magnetism and Magnetic Materials*, *183*(3), 365–374. https://doi.org/10.1016/S0304-8853(97)01097-4

Piper, J. D. A., Atkinson, D., Norris, S., & Thomas, S. (1991). Palaeomagnetic study of the Derbyshire lavas and intrusions, central England: Definition of Carboniferous apparent polar wander. *Physics of the Earth and Planetary Interiors*, *69*(1–2), 37–55. https://doi.org/10.1016/0031-9201(91)90152-8

Piper, J. D. A., & Crowley, S. F. (1999). Palaeomagnetism of (Palaeozoic) Peel Sandstones and Langness Conglomerate Formation, Isle of Man: Implications for the age and regional diagenesis of Manx red beds. In N. H. Woodcock, D. G. Quirk, W. R. Fitches, & R. P. Barnes (Eds.), In *Sight of the suture: the Palaeozoic geology of the Isle of Man in its Iapetus Ocean context*, *Geological Society, London, Special Publications* (Vol. 160, pp. 213–225). Geological Society.

Pointon, M. A., Chew, D. M., Ovtcharova, M., Sevastopulo, G. D., & Delcambre, B. (2014). High-precision U–Pb zircon CA-ID-TIMS dates from western European late Viséan bentonites. *Journal of the Geological Society*, *171*(5), 649–658. https://doi.org/10.1144/jgs2013-106

Rex, G. M., & Scott, A. C. (1987). The sedimentology, palaeoecology and preservation of the Lower Carboniferous plant deposits at Pettycur, Fife, Scotland. *Geological Magazine*, *124*(1), 43–66. https://doi.org/10.1017/S0016756800015776

Roberts, A. P. (2015). Magnetic mineral diagenesis. *Earth-Science Reviews*, *151*, 1–47. https://doi.org/10.1016/j.earscirev.2015.09.010

Rose, W. C. C., & Dunham, K. C. (1977). *Geology and hematite deposits of South Cumbria, Economic Memoir of the Geological Survey of Great Britain, Sheets 58 and part of 48*. HMSO.

Rother, K., & Storetvedt, K. M. (1991). Polyphase magnetization in Lower Carboniferous rocks of S. Scotland: Palaeomagnetic and tectonic considerations. *Physics of the Earth and Planetary Interiors*, *67*(3–4), 251–267. https://doi.org/10.1016/0031-9201(91)90022-A

Rowe, J., Turner, P., & Burley, S. (1998). Palaeomagnetic dating of the west Cumbrian hematite deposits and implications for their mode of formation. *Proceedings of the Yorkshire Geological Society*, *52*(1), 59–71. https://doi.org/10.1144/pygs.52.1.59

Rygel, M. C., Fielding, C. R., Frank, T. D., & Birgenheier, L. P. (2008). The magnitude of Late Paleozoic glacioeustatic fluctuations: A synthesis. *Journal of Sedimentary Research*, *78*(8), 500–511. https://doi.org/10.2110/jsr.2008.058

Setiabudidaya, D., Piper, J. D. A., & Shaw, J. (1994). Palaeomagnetism of the (Early Devonian) Lower Old Red Sandstones of South Wales: Implications to Variscan overprinting and differential regional rotations. *Tectonophysics*, *231*(4), 257–280. https://doi.org/10.1016/0040-1951(94)90038-8

Sinnesael, M., De Vleeschouwer, D., Zeeden, C., Batenburg, S. J., Da Silva, A. C., de Winter, N. J., et al. (2019). The Cyclostratigraphy Intercomparison Project (CIP): Consistency, merits and pitfalls. *Earth-Science Reviews*, *199*, 102965. https://doi.org/10.1016/j.earscirev.2019.102965

Stephenson, A. (1993). Three-axis static alternating field demagnetization of rocks and the identification of natural remanent magnetization, gyroremanent magnetization, and anisotropy. *Journal of Geophysical Research*, *98*(B1), 373–381. https://doi.org/10.1029/92JB01849

Strank, A. R. E. (1985). The Dinantian biostratigraphy of a deep borehold near Eyam, Derbyshire. *Geological Journal*, *20*(3), 227–237. https://doi.org/10.1002/gj.3350200304

Thallner, D., Shcherbakova, V. V., Bakhmutov, V. G., Shcherbakov, V. P., Zhidkov, G. V., Poliachenko, I. B., & Biggin, A. J. (2022). New palaeodirections and palaeointensity data from extensive profiles through the Ediacaran section of the Volyn Basalt Province (NW Ukraine). *Geophysical Journal International*, *231*(1), 474–492. https://doi.org/10.1093/gji/ggac186

Torsvik, T. H., Lyse, O., Atteras, G., & Bluck, B. J. (1989). Palaeozoic palaeomagnetic results from Scotland and their bearing on the British apparent polar wander path. *Physics of the Earth and Planetary Interiors*, *55*(1–2), 93–105. https://doi.org/10.1016/0031-9201(89)90236-7

Torsvik, T. H., Van der Voo, R., Preeden, U., Mac Niocaill, C., Steinberger, B., Doubrovine, P. V., et al. (2012). Phanerozoic polar wander, palaeogeography and dynamics. *Earth-Science Reviews*, *114*(3–4), 325–368. https://doi.org/10.1016/j.earscirev.2012.06.007

Turner, P. (1975). Depositional magnetization of Carboniferous limestones from the Craven Basin of northern England. *Sedimentology*, *22*(4), 563–581. https://doi.org/10.1111/j.1365-3091.1975.tb00246.x

Turner, P., Metcalfe, I., & Tarling, D. H. (1979). Palaeomagnetic studies of some Dinantian limestones from the Craven Basin and a contribution to Asbian magnetostratigraphy. *Proceedings of the Yorkshire Geological Society*, *42*(3), 371–396. https://doi.org/10.1144/pygs.42.3.371

Turner, P., & Tarling, D. H. (1975). Implications of new palaeomagnetic results from the Carboniferous System of Britain. *Journal of the Geological Society*, *131*(5), 469–488. https://doi.org/10.1144/gsjgs.131.5.0469

Utting, J., Giles, P. S., & Dolby, G. (2010). Palynostratigraphy of Mississippian and Pennsylvanian rocks, Joggins area, Nova Scotia and New Brunswick, Canada. *Palynology*, *34*(1), 43–89. https://doi.org/10.1080/01916121003620569

van der Boon, A., Biggin, A. J., Thallner, D., Hounslow, M. W., Bono, R., Nawrocki, J., et al. (2022). A persistent non-uniformitarian paleomagnetic field in the Devonian? *Earth-Science Reviews*, *231*, 104073. https://doi.org/10.1016/j.earscirev.2022.104073

Wakefield, O., Waters, C. N., & Smith, N. J. P. (2016). *Carboniferous stratigraphical correlation and interpretation in the Irish Sea, British Geological Survey commisioned report, (Rep. CR/16/040)*. British Geological Survey. Retrieved from nora.nerc.ac.uk/id/eprint/516783/

Walden, J. (1999). Remanence measurements. In J. Walden, F. Oldfield, & J. Smith (Eds.), *Environmental magnetism: A practical guide, quaternary research association, technical guide* (Vol. 6, pp. 63–88). Quaternary Research Association.

Walden, J., & White, K. (1997). Investigation of the controls on dune colour in the Namib Sand Sea using mineral magnetic analyses. *Earth and Planetary Science Letters*, *152*(1–4), 187–201. https://doi.org/10.1016/S0012-821X(97)00154-4

Waters, C. N., Burgess, I. C., Cózar, P., Holliday, D. W., & Somerville, I. D. (2021). Reappraisal of Arundian–Asbian successions of the Great Scar Limestone Group across northern England. *Proceedings of the Yorkshire Geological Society*, *63*(4). https://doi.org/10.1144/pygs2021-002

Waters, C. N., Cózar, P., Somerville, I. D., Haslam, R. B., Millward, D., & Woods, M. (2017). Lithostratigraphy and biostratigraphy of Lower Carboniferous (Mississippian) carbonates of the southern Askrigg Block, North Yorkshire, UK. *Geological Magazine*, *154*(2), 305–333. https://doi.org/10.1017/S0016756815000989

Waters, C. N., Dean, M. T., Jones, N. S., & Somerville, I. D. (2011a). Cumbria and the northern Pennines. In C. N. Waters, I. D. Somerville, N. S. Jones, C. J. Cleal, J. D. Collinson, R. A. Waters, et al. (Eds.), *A revised correlation of Carboniferous rocks in the British Isles* (pp. 82–88). Geological Society of London.

Waters, C. N., Glover, B. W., & Powell, J. H. (1994). Structural synthesis of S Staffordshire, UK: Implications for the Variscan evolution of the Pennine Basin. *Journal of the Geological Society*, *151*(4), 697–713. https://doi.org/10.1144/gsjgs.151.4.0697

Waters, C. N., Jones, N. S., Collinson, J. D., & Besly, B. (2011b). Peak District and north Staffordshire. In C. N. Waters, I. D. Somerville, N. S. Jones, C. J. Cleal, J. D. Collinson, R. A. Waters, et al. (Eds.), *A revised correlation of Carboniferous rocks in the British Isles* (pp. 66–73). Geological Society of London.

Watson, G. S., & Enkin, R. J. (1993). The fold test in paleomagnetism as a parameter estimation problem. *Geophysical Research Letters*, *20*(19), 2135–2137. https://doi.org/10.1029/93GL01901

Wilkinson, J. J., Vowles, K., Muxworthy, A. R., & Mac Niocaill, C. (2017). Regional remagnetization of Irish Carboniferous carbonates dates Variscan orogenesis, not Zn-Pb mineralization. *Geology*, *45*, 747–750. https://doi.org/10.1130/G39032.1

Wilson, R. L., & Everitt, C. W. F. (1963). Thermal demagnetization of some Carboniferous lavas for palaeomagnetic purposes. *Geophysical Journal International*, *8*(2), 149–164. https://doi.org/10.1111/j.1365-246X.1963.tb06279.x

Wright, V. P. (1994). Paleosols in shallow marine carbonate sequences. *Earth-Science Reviews*, *35*(4), 367–395. https://doi.org/10.1016/0012-8252(94)90002-7

Wright, V. P., Vanstone, S. D., & Marshall, J. D. (1997). Contrasting flooding histories of Mississippian carbonate platforms revealed by marine alteration effects in palaeosols. *Sedimentology*, *44*(5), 825–842. https://doi.org/10.1046/j.1365-3091.1997.d01-51.x

References From the Supporting Information

Abplanalp, J. M., Isaacson, P. E., Batt, L. S., & Pope, M. C. (2009). Conodont biostratigraphy of Chesterian strata (Late Mississippian–Early Pennsylvanian), east central Idaho and southwestern Montana. *Mountain Geologist*, *46*, 89–104.

Batt, L. S., Montañez, I. P., Isaacson, P., Pope, M. C., Butts, S. H., & Abplanalp, J. (2007). Multi-carbonate component reconstruction of mid-Carboniferous (Chesterian) seawater $\delta^{13}C$. *Palaeogeography, Palaeoclimatology, Palaeoecology*, *256*(3–4), 298–318. https://doi.org/10.1016/j.palaeo.2007.02.049

Besly, B. M., & Turner, P. (1983). Origin of red beds in a moist tropical climate (Etruria Formation, Upper Carboniferous, UK. In R. C. L. Wilson (Ed.), *Residual deposits: Surface related weathering processes and materials*, *Geological Society, London, Special Publications* (Vol. 11, pp. 131–147). Geological Society.

Buggisch, W., Joachimski, M. M., Sevastopulo, G., & Morrow, J. R. (2008). Mississippian $\delta^{13}C_{carb}$ and conodont apatite $\delta^{18}O$ records—Their relation to the Late Palaeozoic Glaciation. *Palaeogeography, Palaeoclimatology, Palaeoecology*, *268*(3–4), 273–292. https://doi.org/10.1016/j.palaeo.2008.03.043

Chen, J., Chen, B., & Montañez, I. P. (2022). Carboniferous isotope stratigraphy. In S. G. Lucas, J. W. Schneider, X. Wang, & S. Nikolaeva (Eds.), *The Carboniferous timescale*, *Geological Society, London, Special Publications* (Vol. 512, pp. 197–211). Geological Society. https://doi.org/10.1144/SP512-2020-72

Conil, R., Groessens, E., & Pirlet, H. (1977). Nouvelle charte stratigraphique du Dinantien type de la Belgique. *Annales de la Societe Geologique du Nord*, *96*, 363–371.

Cramer, B. D., & Jarvis, I. (2020). Carbon isotope stratigraphy. In F. M. Gradstein, J. G. O. M. D. Schmitz, & G. M. Ogg (Eds.), *Geologic time scale 2020* (pp. 309–343). Elsevier. https://doi.org/10.1016/B978-0-12-824360-2.00011-5

Dyer, B., Maloof, A. C., & Higgins, J. A. (2015). Glacioeustasy, meteoric diagenesis, and the carbon cycle during the Middle Carboniferous. *Geochemistry, Geophysics, Geosystems*, *16*(10), 3383–3399. https://doi.org/10.1002/2015GC006002

Fisher, N. I., Lewis, T., & Embleton, B. J. (1993). *Statistical analysis of spherical data*. Cambridge University Press.

Horbury, A. D., & Adams, A. E. (1989). Meteoric phreatic diagenesis in cyclic late Dinantian carbonates, northwest England. *Sedimentary Geology*, *65*(3–4), 319–344. https://doi.org/10.1016/0037-0738(89)90032-8

Iosifidi, A. G., & Khramov, A. N. (2013). Paleomagnetism of Devonian and Carboniferous sedimentary rocks of Spitsbergen: To the Paleozoic history of the Barents-Kara basin framing. *Izvestiya - Physics of the Solid Earth*, *49*(5), 725–742. https://doi.org/10.1134/S1069351313040034

Iosifidi, A. G., & Mikhailova, V. A. (2017). Paleomagnetism of Carboniferous formations of the Russian platform: Reinvestigation of old collections. *Izvestiya - Physics of the Solid Earth*, *53*(3), 461–476. https://doi.org/10.1134/S1069351317020069

Iosifidi, A. G., Mikhailova, V. A., Popov, V. V., Sergienko, E. S., Danilova, A. V., & Otmas, N. M. (2018). The Carboniferous of the Moscow syneclise: Paleomagnetic data. *Izvestiya - Physics of the Solid Earth*, *54*(1), 163–177. https://doi.org/10.1134/S1069351318010081

Iosifidi, A. G., Mikhailova, V. A., Popov, V. V., Sergienko, E. S., Danilova, A. V., Otmas, N. M., & Zhuravlev, A. V. (2019). Carboniferous of the Russian platform: Paleomagnetic data. In D. Nurgaliev, V. Shcherbakov, A. Kosterov, & S. Spassov (Eds.), *Recent advances in rock magnetism, environmental magnetism & paleomagnetism* (pp. 37–54). Springer. https://doi.org/10.1007/978-3-319-90437-5_4

Kent, J. T., Briden, J. C., & Mardia, K. V. (1983). Linear and planar structure in ordered multivariate data as applied to progressive demagnetization of palaeomagnetic remanence. *Geophysical Journal International*, *75*(3), 593–621. https://doi.org/10.1111/j.1365-246X.1983.tb05001.x

Liu, C., Jarochowska, E., Du, Y., Vachard, D., & Munnecke, A. (2015). Microfacies and carbon isotope records of Mississippian carbonates from the isolated Bama Platform of Youjiang Basin, South China: Possible responses to climate-driven upwelling. *Palaeogeography, Palaeoclimatology, Palaeoecology*, *438*, 96–112. https://doi.org/10.1016/j.palaeo.2015.07.048

Liu, Q., Yu, Y., Torrent, J., Roberts, A. P., Pan, Y., & Zhu, R. (2006). Characteristic low-temperature magnetic properties of aluminous goethite [α-(Fe, Al) OOH] explained. *Journal of Geophysical Research*, *111*(B12), B12S34. https://doi.org/10.1029/2006JB004560

Makhlina, M. K., Vdovenko, M. V., Alekseev, A. S., Byrsheva, T. V., Donakova, L. M., Zhulitova, V. E., et al. (1993). Early Carboniferous of the Moscow Synclise and Voronezh anteclise. Rossiiskaya Akademiya Nauk, Poskovskoe Obshchestvo Ispytatelei Pridory. *Komitet po Geologii i Ispolzonalniyu Nedr Pri Pravitelstve Rossiikoi Federalii* (p. 223). Nauka. [in Russian].

Mamet, B. L., Skipp, B., Sando, W. J., & Mapel, W. J. (1971). Biostratigraphy of upper Mississippian and associated Carboniferous rocks in south-central Idaho. American Association of Petroleum Geologists. *Bulletin*, *55*, 20–33.

Meijers, M. J., Hamers, M. F., van Hinsbergen, D. J., van der Meer, D. G., Kitchka, A., Langereis, C. G., & Stephenson, R. A. (2010). New late Paleozoic paleopoles from the Donbas Foldbelt (Ukraine): Implications for the Pangea A vs. B controversy. *Earth and Planetary Science Letters*, *297*(1–2), 18–33. https://doi.org/10.1016/j.epsl.2010.05.028

Michalski, K., & Lewandowski, M. (2004). Palaeomagnetic results from the Middle Carboniferous rocks of the Hornsund region, southern Spitsbergen: Preliminary report. *Polish Polar Research*, *25*, 169–182.

Middleton, M., & Schmidt, P. W. (1982). Paleothermometry of the Sydney Basin. *Journal of Geophysical Research*, *87*(B7), 5351–5359. https://doi.org/10.1029/JB087iB07p05351

Popov, V. V., Sergienko, E. S., Iosifidi, A. G., & Mikhailova, V. A. (2016). Paleomagnetic studies of the reference section of the Lower Carboniferous of Msta River. In *11th international conference "Problems of geocosmos", Book of abstracts, St. Petersburg, Petrodvorets, October 3–7* (p. 165). SPSU.

Pullaiah, G., Irving, E., Buchan, K. L., & Dunlop, D. J. (1975). Magnetization changes caused by burial and uplift. *Earth and Planetary Science Letters*, *28*(2), 133–143. https://doi.org/10.1016/0012-821X(75)90221-6

Roberts, R. J., Torsvik, T. H., Andersen, T. B., & Rehnstrom, E. F. (2003). The Early Carboniferous Magerøy dykes, northern Norway: Palaeomagnetism and palaeogeography. *Geological Magazine*, *140*(4), 443–451. https://doi.org/10.1017/S0016756803008082

Smirnov, A. V., & Tarduno, J. A. (2000). Low-temperature magnetic properties of pelagic sediments (Ocean Drilling Program Site 805C): Tracers of maghemitization and magnetic mineral reduction. *Journal of Geophysical Research*, *105*(B7), 16457–16471. https://doi.org/10.1029/2000JB900140

Watts, D. R. (1985). Palaeomagnetism of the Lower Carboniferous Billefjorden Group, Spitsbergen. *Geological Magazine*, *122*(4), 383–388. https://doi.org/10.1017/S0016756800031824

Westphal, M., Edel, J. B., Kadzialko-Hofmokl, M., Jelenska, M., & Grocholski, A. (1987). Paleomagnetic study of Upper Carboniferous volcanics from Sudetes (Poland). *Journal of Geophysics*, *61*, 90–96. Retrieved from https://journal.geophysicsjournal.com/JofG/article/view/125